A ground penetrating radar study of water table elevation in a portion of Wisconsin's central sand plain. [DNR-050] 1988

Bohling, Geoffrey C.
[s.l.]: [s.n.], 1988

A Ground Penetrating Radar Study of Water Table Evelation in a Portion of Wisconsin's Central Sand Plain.

G.C. Bohling

A GROUND PENETRATING RADAR STUDY OF WATER TABLE ELEVATION IN A PORTION OF WISCONSIN'S CENTRAL SAND PLAIN

by

Geoffrey C. Bohling

A thesis submitted in partial fulfillment of the requirements for the degree of

Master of Science
(Geology)

at the

UNIVERSITY OF WISCONSIN-MADISON

1988

Approved Mary P Anderson

Mary P. Anderson
Professor
June 24, 1988

ABSTRACT

Contamination of groundwater by agricultural chemicals in the Central Sand Plain has prompted studies of groundwater flow in this region. Because the groundwater system is particularly susceptible to contamination in areas where groundwater recharge occurs, identification of recharge zones can contribute significantly to the effective management of agricultural chemical use. An accurate map of water table elevation (groundwater head) is crucial to identifying the distribution of recharge.

This project tests the reliability of ground penetrating radar (GPR) as a tool for obtaining high-resolution maps of water table elevation. GPR surveys were performed in the summer and fall of 1987 in an approximately nine square mile area in the Central Sand Plain with a fairly dense set of existing water table observation wells. GPR is a geophysical instrument which transmits an electromagnetic pulse into the ground and records the return times of pulses reflected from subsurface interfaces, producing a profile of return time versus horizontal distance as the radar is pulled along the ground. In order to test the reliability of GPR as a water table reconnaissance tool, sparse subsets of wells in the area are used to calibrate the radar and water table depths obtained from these calibrations are compared to known water table depths in the remaining wells. Thus, the study tests whether GPR can be used to help produce an accu-

rate water table map when only a few observation wells exist.

Three wells are the minimum necessary to obtain an estimate of uncertainty in calibration parameters, specifically the radar signal velocity in the subsurface materials and the return time correction factor. Results indicate that, in the study area, three calibrating wells are adequate to give a correlation of 0.99 and a root mean squared deviation of about 1 foot between radar-predicted and observed water table depths. If several wells distributed throughout a region of interest do yield consistent calibration results, radar can be used to produce a map of water table elevation in that region.

Attempts to model the distribution of groundwater recharge and discharge in the study area were not very successful. Model results appear to be highly dependent on the technique employed to interpolate a water table map from either the well or radar data. However, a water table map produced from radar data in an area with sparse well coverage would still be useful for guiding further hydrogeological work in that area.

ACKNOWLEDGMENTS

Most of the funding for this project was provided by a federal grant administered through the Water Resources Center of the University of Wisconsin-Madison. Additional funding was provided by the Wisconsin Department of Natural Resources.

I would like to thank the members of my committee for their suggestions for the project and their comments on this thesis. Collectively my committee members represent an intimidating level of expertise on all aspects of my project. Prof. Charles Bentley made helpful comments on the presentation of radar theory in Chapter III. Prof. Ken Potter, of the Department of Civil and Environmental Engineering, assisted with instruction in statistical techniques and commented on the analysis presented in Chapter V. Prof. Mary Anderson, my advisor, provided insightful comments on the entire thesis, especially the hydrogeological aspects and the writing.

I would like to thank the two people who have had the most influence on my education in hydrogeology. Dr. Carl McElwee, my supervisor at the Kansas Geological Survey, sparked my interest in hydrogeology and instructed me in the mathematical intricacies of groundwater modeling. I look forward to working with him again. Prof. Mary Anderson provided an excellent overview of the world of hydrogeology and the

place of modeling within it.

Mary Stoertz, my fellow graduate student and friend, provided much guidance in this project. She and her husband, Doug Green, were also good neighbors. They have contributed greatly to making our two years here in Madison enjoyable and rewarding.

George Kraft of the Department of Soil Science provided me with data and access to his field area. I wish him success in his work.

I would like to thank my fellow hydrogeology graduate students. My interaction with them has been an important part of my education. I would especially like to thank my office mate and friend, Tamie Weaver. My talks with her have helped me through the times of discouragement.

I would like to thank Dr. Raimo Sutinen for his instruction in the use of ground penetrating radar and Mike Lemcke of the Wisconsin Geological and Natural History Survey for his patience with my questions and requests. I would also like to thank Tom Osborne of the Central Wisconsin Groundwater Center and the students of the University of Wisconsin-Stevens Point who provided field help.

Finally, I would like to thank my wife, Gwen, for her love and encouragement and my son, Christopher, for the joy and richness he has brought to our lives.

TABLE OF CONTENTS

LIST OF FIGURES

LIST OF TABLES

I. INTRODUCTION: MOTIVATION AND OBJECTIVES

A. Contamination and Recharge

Incidents of contamination of groundwater by agricultural chemicals in Wisconsin's Central Sand Plain (Figure 1) have led to increased interest in protecting groundwater in this area. In particular, contamination by the pesticide aldicarb has received much attention in the past few years. Aldicarb, marketed by Rhone-Poulenc Agricultural Company (formerly Union Carbide Agricultural Products Division) under the trade name Temik, is a water-soluble, soil-incorporated systemic pesticide. In Wisconsin's Central Sand Plain it has been used primarily on potatoes to control the Colorado potato beetle and the golden nematode (Harkin et al., 1986).

Although it is only one of a number of agricultural chemicals that could potentially contaminate groundwater, aldicarb has become the subject of particular attention for at least two reasons: 1) Its initial detection in drinking water wells on Long Island, New York, in the summer of 1979 received much publicity and generated a number of studies of aldicarb's contamination potential. For a summary of events related to aldicarb contamination on Long Island, see Wartenberg (1988). 2) Aldicarb is viewed as a worst case contaminant because it is highly soluble in water and it is poorly adsorbed by soil matrix material (Rothschild et al., 1982). Harkin

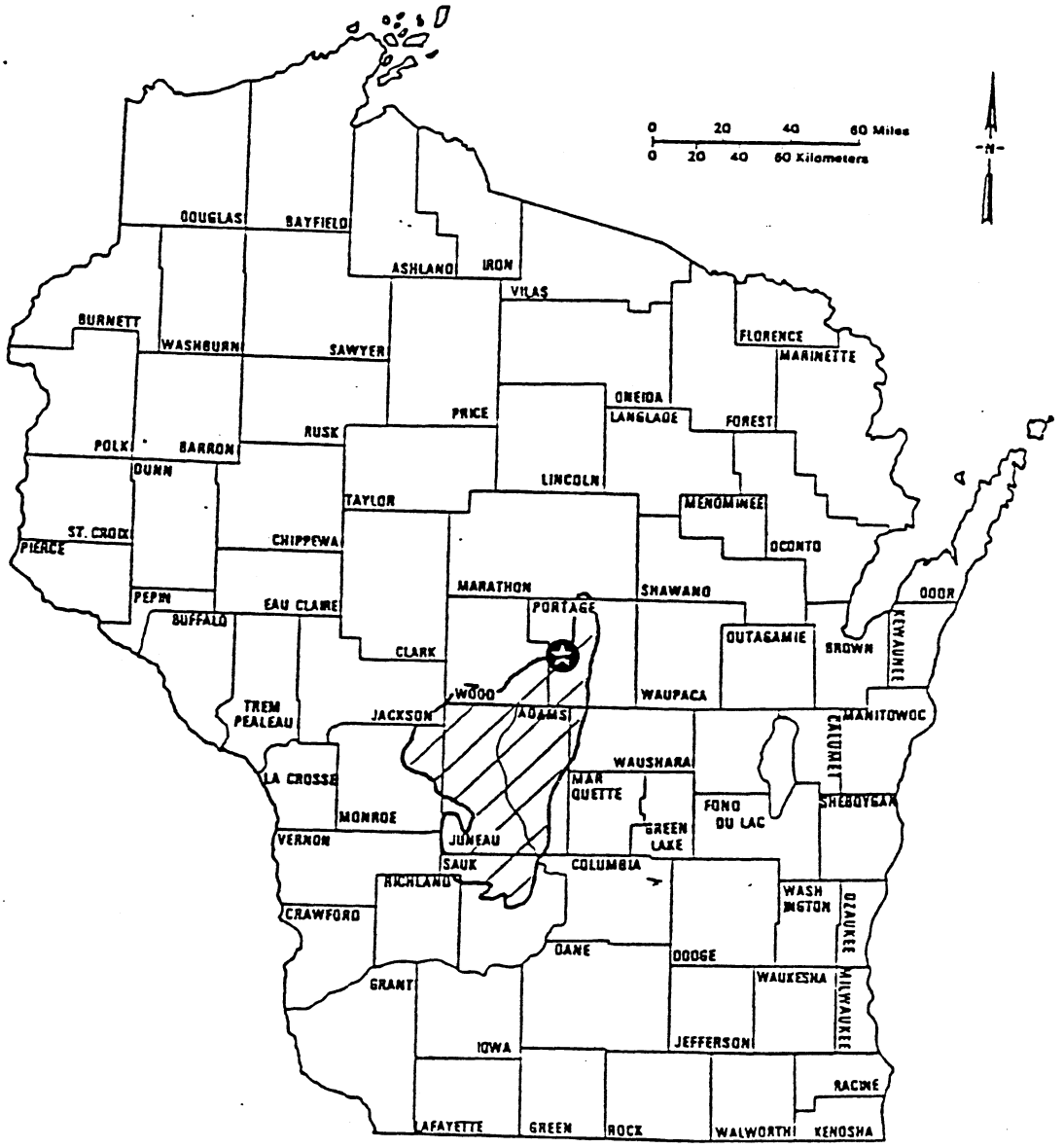

Figure 1. Location of study area (star) in Wisconsin's Central Sand Plain (dashed).

et al. (1986), conclude that " regardless of application rate, timing and frequency, residues of aldicarb are leached beyond the rooting zone of potatoes grown in irrigated sandy soils into underlying groundwater."

Aldicarb was first detected in groundwater in Wisconsin's Central Sand Plain in 1980 (Wartenberg, 1988; Harkin et al., 1986). The Wisconsin Department of Agriculture, Trade and Consumer Protection has responded by declaring a moratorium on aldicarb use within a one-mile radius around each drinking water well showing aldicarb concentrations higher than the enforcement standard of 10 ppb. This regulation strategy could be made more effective by delineating those areas which are particularly sensitive and those areas which are less sensitive to contamination and regulating the use of aldicarb (and other agricultural chemicals) based on that knowledge. Rothschild et al. (1982, p. 444), conclude, " Delineation of sensitive areas should be based on the potential for aldicarb to reach the water table and on the potential for the chemical to persist after it has entered the ground-water system."

Recent investigators (Stoertz, 1985; Faustini, 1985) attempted to map the distribution of areas of groundwater recharge and discharge in the Buena Vista Groundwater Basin in the Central Sand Plain. Recharge areas are those areas in a drainage basin where the net flux of water near the water table is downward (into the groundwater flow system) and discharge areas are those where the net flux of water near the water table

is upward (Freeze and Cherry, 1979, p. 194). One would expect that the groundwater system would be more sensitive to contamination in recharge areas than in discharge areas. This is indeed true, but not necessarily for the most obvious reasons. Stoertz (1985, pp. 13-15) discusses the fact that groundwater recharge and discharge are transient processes and that recharge may occur in what is predominantly a discharge area (and vice-versa). Stoertz (1985, pp. 16-17) also pointed out that upward flux of water across the water table does not necessarily occur in a discharge area, especially if the water is discharging laterally through a bank or bluff to a lake or stream. Therefore, a discharge area is not entirely protected from contamination, since soil water may flow downward to the water table in such an area. Moreover, Harkin et al. (1986, p. 15), reported that the movement of aldicarb from the root zone of plants to the water table is controlled by soil processes which produce concentration distributions that are erratic both in space and in time, even given uniform application rates at the surface. It appears that soil processes are more important in determining whether a chemical used on an agricultural field will reach the water table than is the location of that field with respect to the groundwater flow system.

However, contaminants which enter the groundwater system in a recharge area will have a longer residence time in the flow system and will affect a much larger portion of the system than those that enter the

system in a discharge area. Therefore, use of an agricultural chemical on a field in a discharge area should have a less detrimental effect on the groundwater system than its use on a field in a recharge area.

B. Objectives

The primary objective of this study is to test the reliability of ground penetrating radar (GPR) as a tool for obtaining high-resolution maps of water table elevation. GPR surveys were performed in the summer and fall of 1987 in a portion of the Central Sand Plain with a fairly dense set of existing water table observation wells. GPR is a geophysical instrument which transmits an electromagnetic pulse into the ground and records the return times of pulses reflected from subsurface interfaces, producing a profile of return time versus horizontal distance as the radar is pulled along the ground. In order to test the reliability of GPR as a water table reconnaissance tool, sparse subsets of wells in the area are used to calibrate the radar and water table depths obtained from these calibrations are compared to known water table depths in the remaining wells. Water table elevation maps produced from observation well data and from the GPR data are also compared. Thus, the study tests whether GPR can be used to help produce an accurate water table map when only a few observation wells exist. The results of these comparisons are presented in Chapter V.

Water table maps can be used to help delineate the distribution of recharge and discharge in a region. In this study, water table maps produced from the GPR surveys were used as input to a mass balance model which calculates a recharge/discharge distribution based on the configuration of the water table. Although these modeling efforts were not very successful, it is possible that a different modeling technique would yield more reasonable results. If so, GPR would be a useful tool for reconnaissance studies of both water table configuration and groundwater recharge/discharge. The recharge modeling results are analyzed in Appendix 1.

Chapter II is a discussion of the geology and hydrogeology of the study area. In Chapter III, relevant aspects of radar theory are presented. The field work for this study is described in Chapter IV.

C. Location of Field Area

A detailed map of the field area is shown in Figure 2. The field area is just southwest of the town of Plover in Portage County. The northern boundary of the study area is the bluff along the Wisconsin River and its adjoining wetlands. A groundwater divide runs through the study area. North of this divide, groundwater flows toward the Wisconsin River. The area south of this divide is part of the Buena Vista Groundwater Basin, studied by Stoertz (1985) and Faustini (1985).

●12 observation well and well number

□4t site of pump test (Weeks and Stangland, 1971)

109 ○ location of boring for grain size analysis

approximate location of groundwater divide

Figure 2. Detailed map of the study area.

In this study, locations of GPR data points and piezometers are expressed in terms of miles east of County Highway F and miles north of Birch Street. County Highway F runs north-south along the western edge of Figure 2, intersecting with State Highway 54 southwest of Love Creek. Birch Street runs along the southern edge of Figure 2. It is named Birch Drive east of Monroe Avenue, which is two miles east of County Highway F. It should also be noted that Drainage Ditch Number 1 runs parallel to and just north of Birch Drive east of Monroe Avenue. West of Monroe Avenue, Drainage Ditch Number 1 flows southwest, away from the study area.

Most of the piezometers in the field area were installed for an ongoing study of aldicarb contamination being carried out by George Kraft of the Department of Soil Science, University of Wisconsin-Madison (Kraft, in preparation). A number of the piezometers in the eastern portion of the area were installed for the previously mentioned study by Harkin et al. (1986) who reported that water samples from a number of these piezometers have had high concentrations of aldicarb residues, some over 100 ppb, and that two domestic wells in the study area have also had aldicarb levels higher than the enforcement standard of 10 ppb.

For the analysis described in Chapter V, water table return times obtained from radar records are compared to water levels observed in those observation wells shown in Figure 2 which are next to roads where

GPR surveys were performed. Of the 27 observation wells shown, 21 are next to roads where surveys were performed and are therefore potential calibration and verification points for the radar study. It is important to point out that most of the " observation wells" shown in Figure 2 are actually the shallowest piezometers in nests of 3 to 5 piezometers screened at different depths in one place. Sixteen of the 27 shallow piezometers shown are in fact observation wells, meaning that the water table intersects the screened interval and thus that the water level actually represents water table elevation. Of the 21 shallow piezometers next to surveyed roads, 12 are actually observation wells. In the remaining nine, water stands between 0.5 and 12 feet above the top of the well screen. It is possible that, due to vertical hydraulic gradients, the water level in piezometers screened below the water table would stand higher or lower than the actual water table elevation. In an actual water table reconnaissance study using GPR, one in which only a few observation wells or piezometers exist in the area, very little or no information concerning vertical gradients would be available.

These 27 shallow piezometers will be referred to as observation wells in this study. Also, the borings for grain size analyses (locations shown in Figure 2) are given the labels of the piezometers which were installed in the auger holes from which the borings were taken.

II. GEOLOGY AND HYDROGEOLOGY OF THE STUDY AREA

A. Introduction

Deposits of glacial outwash sand approximately 70 feet thick overlie nearly impermeable crystalline bedrock over most of the study area. Apparently some sandstone overlies the crystalline bedrock and underlies the outwash in the northern portion of the study area (Kraft, in preparation). The thickness and hydraulic properties of the glacial sediments influence the distribution of recharge in the area.

B. Elevation and Nature of Bedrock

In an east-west cross section through the study area, approximately along the line of Forest Drive (Figure 2), Clayton (1986, Plate 2) shows Precambrian crystalline bedrock underlying the outwash sediments. He shows the top of the bedrock sloping from about 1010 feet above sea level at the western end of the study area (beneath Love Creek) to about 980 feet above sea level at the eastern end of the study area. This bedrock can be considered practically impermeable relative to the highly permeable glacial outwash sands. Clayton also shows about eight feet of " older hillslope deposits" overlying the Precambrian rock. These deposits are derived from the Precambrian rock and contain 3 to 35 percent clay-sized particles (Clayton, 1986, p. 3). Since this clayey residuum should also be considerably less permeable than the overlying sands, the top of the

residuum is considered to be the impermeable base of the glacial outwash aquifer.

Kraft's detailed borings in the study area (Kraft, in preparation) seem to contradict the information shown in Clayton's study. Kraft's map of the elevation of the top of the Precambrian (actually the top of the clayey residuum) shows a topographic high of 1015 feet above sea level at observation well number 125, in the eastern third of the study area. From this high point, Kraft shows the Precambrian surface sloping away to the south, west and northwest. A value of 978 feet above sea level is recorded at observation well number 123 (Figure 2).

In addition, Kraft shows a pronounced slope in the Precambrian bedrock surface northwest from observation well 125, with an elevation of 955 feet above sea level recorded near observation well number 104 (Figure 2), next to the river bluff. Kraft reports that sandstone occurs between the Precambrian surface and the outwash sand in the area north of Highway 54, possibly coinciding with the area of steep dip in the Precambrian surface. Kraft also reports that the sandstone did not offer a great deal of resistance to drilling and that samples of it consisted of loose grains. It is impossible to determine the degree of cementation of the sandstone, however, since the samples were obtained during augering. Therefore, it is difficult to estimate the magnitude of the permeability contrast between the sandstone and the glacial sediments. The elevation of the top of the

sandstone is about 1000 feet above sea level. An earlier map of bedrock (Weeks and Stangland, 1971; modified by Faustini, 1985) also shows sandstone occurring north of Highway 54 in the study area.

C. Glacial Outwash Sand

The glacial outwash sand in the area is composed primarily of sediments that were deposited in glacial Lake Wisconsin during the Almond and Hancock phases of Wisconsin Glaciation (Clayton, 1986). Associated stream sediments may occur in the northeastern corner of the study area. The sediments in the area correspond to lithologic units 3 and 4 described by Brownell (1986). Brownell reports that these units are composed predominantly of moderately-well-sorted and moderately-sorted medium sand. Figures 3, 4 and 5 show grain size distributions for the sand fractions of samples taken at different depths in borings 103, 107 and 109 in the study area (Figure 2). The data are from Kraft (in preparation). The samples are composed primarily of medium sand with some coarse sand and are predominantly moderately-well-sorted, except for the samples from boring 109, which are predominantly well-sorted. There appear to be no consistent trends with depth.

The land surface is fairly level in the area, ranging in elevation from about 1060 to about 1070 feet above sea level. The saturated thickness of the aquifer is controlled by the elevation of the water table and the

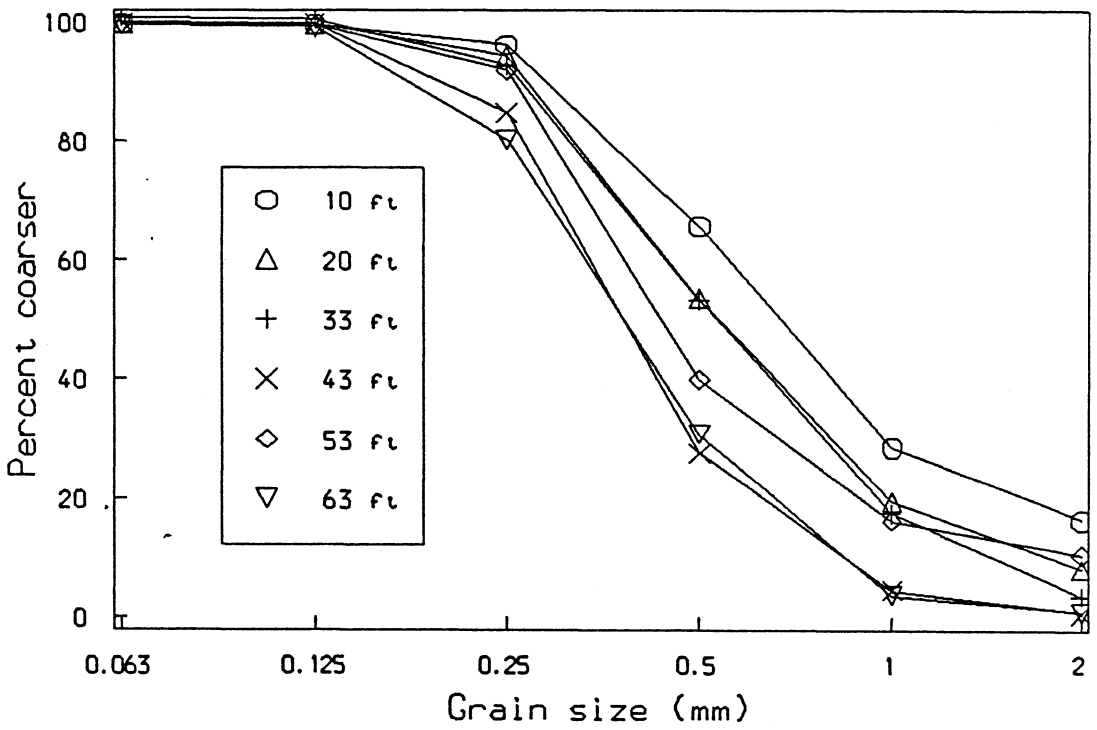

Figure 3. Sediment grain size distributions with depth for boring 103.

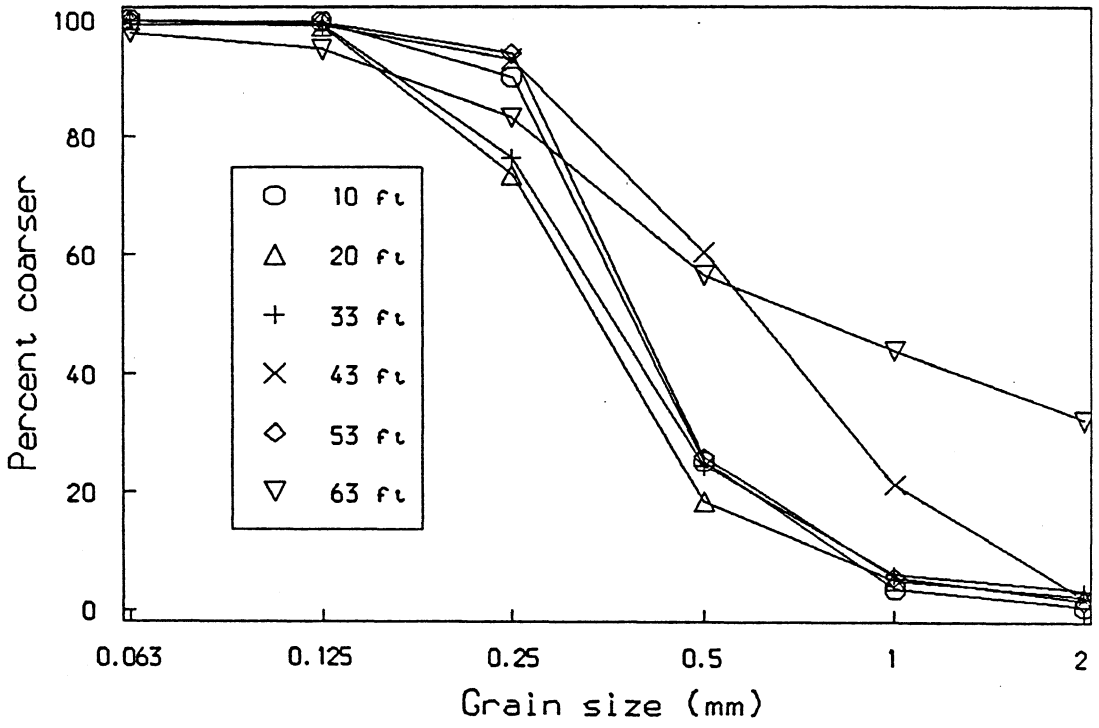

Figure 4. Sediment grain size distributions with depth for boring 107.

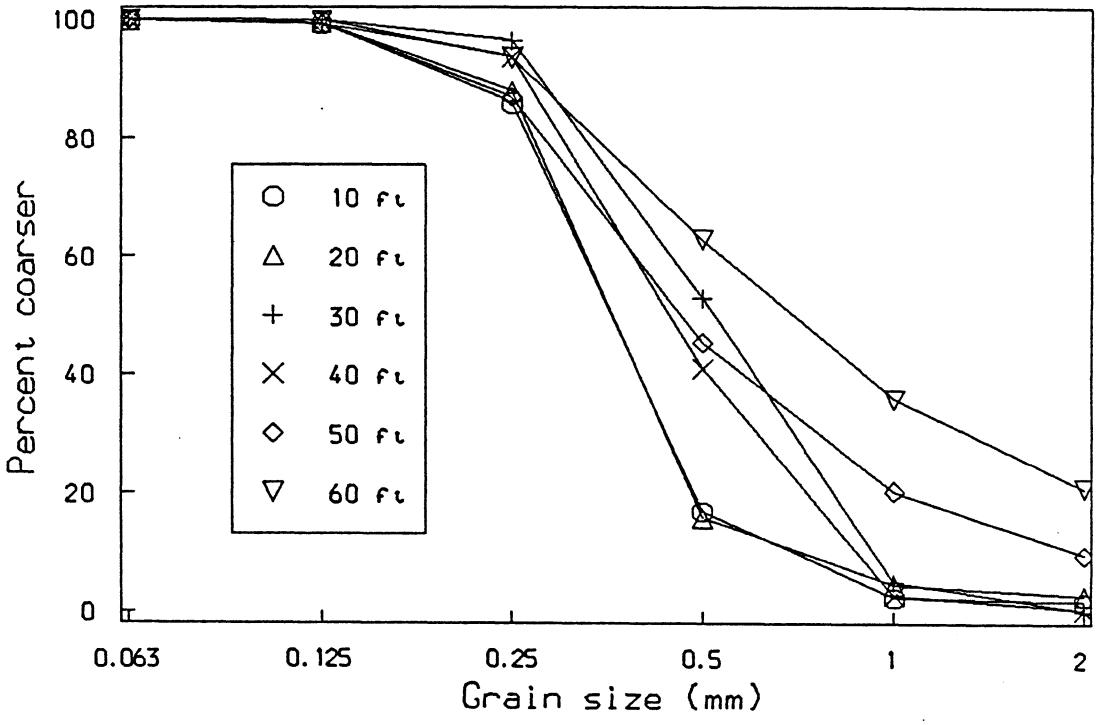

Figure 5. Sediment grain size distributions with depth for boring 109.

elevation of the bottom of the outwash. The water table slopes from an elevation of about 1060 feet in the southern part of the study area to about 1040 feet near the river bluff. The saturated thickness of the aquifer ranges from about 70 feet in the southern part of the study area to about 40 feet near the river bluff (Kraft, in preparation). The saturated thickness and the hydraulic conductivity of the sediments determine the ability of the aquifer to transmit water laterally.

A pump test in the central part of the study area (Figure 2) yielded a hydraulic conductivity for the outwash of 320 ft/day, or 0.11 cm/s (Weeks, 1969; Weeks and Stangland, 1971, p. 24). This is somewhat high compared to other pump test results in the sand plain area, apparently because the sediment is somewhat coarser in the study area than it is elsewhere in the sand plain (Weeks and Stangland, 1971, p. 25). The pump test results were also used to calculate a ratio of horizontal to vertical hydraulic conductivity of 7. Results of slug tests in and near observation well number 1 (Figure 2) give an average hydraulic conductivity of 0.048 cm/s (Kraft, in preparation). Slug tests typically give a lower hydraulic conductivity than do pump tests (e.g., see Muldoon, 1987), presumably because pump tests sample a larger portion of the aquifer material and therefore incorporate the effects of coarser lenses or beds. Therefore, this discrepancy in results is not too surprising.

D. Water Table Fluctuations

In this study the water table is assumed to be at a steady state configuration. Freeze and Cherry (1979, p. 194) state that assumptions of steady state can be considered valid for a basin if annual water table fluctuations are small compared to the saturated thickness of the aquifer and if the relative configuration of the water table remains the same throughout the year. This definition of steady state can be applied to any period being modeled, assuming that the water table has equilibrated to the prevailing conditions for that period. In other words, one could use water table maps from different seasons to produce a recharge map for each season, assuming that prevailing recharge/discharge conditions remain fairly constant throughout each season and that the water table equilibrates quickly to existing stresses.

Because the outwash sands in the study area are so permeable, the water table does equilibrate quickly to existing conditions. Moreover, except under the influence of pumping, the relative water table configuration in the Central Sand Plain remains quite constant throughout the year (Karnauskas, 1977; Holt, 1965). In other words, one could use a water table map from any time in the year to get an idea of the distribution of recharge and discharge areas, although the magnitudes of recharge calculated might vary seasonally.

The data presented in this study were obtained during October and

early November of 1987. During this period, the temporal variation in water levels in most piezometers in the study area was no more than a few hundredths to about a tenth of a foot. Since the growing season was over, the effects of pumping were negligible. Therefore, the water table maps shown in this report can be assumed to represent steady state conditions for the fall of 1987.

III. RADAR THEORY AND HYDROGEOLOGICAL APPLICATIONS

A. Introduction

The aspects of radar theory and performance considerations which must be taken into account when applying GPR to groundwater studies are presented in this chapter. The most important factors affecting results of GPR surveys of the water table are the propagation velocity, attenuation and resolution of the radar signal in the subsurface materials and the strength of the water table as a reflector of electromagnetic energy. All of these factors are influenced by the characteristics of the initial radar pulse and by the electromagnetic properties of the subsurface materials. Because the radar signal is composed of many different frequencies of electromagnetic energy and because the electromagnetic properties of earth materials are frequency-dependent, the analysis of radar signal propagation is, in general, complex. However, in the range of frequencies employed by commercially available GPR units (about 1 to 1000 MHz) simplifying assumptions can be applied to this analysis. These assumptions are employed in the following discussion. For discussion of the more detailed aspects of radar signal propagation, see King and Smith (1981) and Ulriksen (1982). The notation used in the following discussion follows that used by King and Smith (1981).

The specifications of the equipment used in this study and other

applications of GPR to hydrogeology also are discussed in this chapter.

B. Constitutive Parameters

In many applications earth materials can be treated as linear dielectrics, meaning that the vector volume density of electrical current and vector volume density of polarization are proportional to the applied electrical field. The proportionality constant relating the vector volume density of current to the electrical field is called the conductivity and is, in general, a complex value, given by

$$\sigma = \sigma' + i\sigma'' . \tag{1}$$

The proportionality constant relating the vector volume density of polarization to the electrical field is $\epsilon - \epsilon_0$ where

$$\epsilon = \epsilon' + i\epsilon'' \tag{2}$$

is the permittivity of the material and $\epsilon_0 = 8.854 \times 10^{-12}$ Farad/m is the permittivity of free space. The relative permittivity, ϵ_r, is a dimensionless parameter defined such that

$$\epsilon = \epsilon_r \epsilon_0. \tag{3}$$

The imaginary portion of the conductivity, σ'', accounts for time lags in conduction response of the material to a time-varying electrical field. Similarly, ϵ'' accounts for time lags in the polarization response of the material (King and Smith, 1981).

In Maxwell's equations (which govern the propagation of elec-

tromagnetic energy) the above parameters appear in the following combinations:

$$\sigma_e = \sigma' + \omega\epsilon'' \tag{4}$$

and

$$\epsilon_e = \epsilon' - \frac{\sigma''}{\omega} \tag{5}$$

where ω is the angular frequency of the electrical field. The parameters defined in equations 4 and 5 are called the real effective conductivity and the real effective permittivity, respectively. The relative real effective permittivity, $\epsilon_{e\,r}$, is defined such that

$$\epsilon_e = \epsilon_{e\,r}\,\epsilon_0. \tag{6}$$

In the following discussion the term " dielectric constant" refers to $\epsilon_{e\,r}$.

C. Signal Propagation Velocity

In most practical applications, the GPR signal can be considered to be a wave packet moving at a velocity of

$$v = \frac{c}{\sqrt{\epsilon_{e\,r}}} \tag{7}$$

where c = the velocity of light in a vacuum (about 1 ft/ns) (Annan and Davis, 1976; Shih et al., 1986; Ulriksen, 1982; Houck, 1984; Wright et al., 1984; Bogorodsky et al., 1985). Over the range of frequencies of commercially available GPR units, σ'' of earth materials is essentially equal to zero, so that $\epsilon_{e\,r}$ is approximately equal to the real part of the relative

permittivity of the material (Horton et al., 1981; Ulriksen, 1982). Experimental data indicate that $\epsilon_{e\,r}$ for a typical clay loam soil is approximately constant for frequencies from 10 MHz to 3000 MHz (King and Smith, 1981). In this study it is assumed that the same is true for the sandy loam soils and sands in the field area, at least over the frequencies in the 3 dB bandwidth of the antenna employed (approximately 40 to 120 MHz).

The radar signal radiates outward and downward into the ground from the antenna. When this signal impinges on a planar interface, such as the water table, most of the incident energy is either transmitted into the layer below the interface or reflected at angles that do not return to the antenna. However, a portion of the energy which strikes the interface at near-normal incidence will be reflected and return to the antenna. The two-way travel time of this return signal is then recorded on a graphic recorder with a scale calibrated in nanoseconds. A profile of return time versus distance is produced as the radar antenna is pulled along the ground surface. This return time profile can be converted to a depth profile according to the formula

$$D = \frac{vt}{2} \tag{8}$$

where D is the depth to a reflector of interest, t is the two-way travel time and v is the average velocity of the radar signal between the ground surface and the reflector. Alternatively, for a profile with multiple layers,

the thickness of each layer can be calculated using the same formula, with v representing the velocity in a given layer and t representing the two-way travel time of the signal in that layer.

Thus, along with radar survey data, the investigator must also obtain an estimate of radar signal velocity in the subsurface materials in order to obtain quantitative depth data. Several means are available for obtaining signal velocities. The simplest method for estimating the signal velocity in a given material is to look up the value of dielectric constant for that material in a table, such as those presented in Ulriksen (1982) and Horton et al. (1981). These tables contain ranges of dielectric constant encountered in the field for a given medium. For example, the dielectric constant for dry sand is given as 4-6 and that for saturated sand as 30. For many materials, these values are fairly accurate. However, in most cases an investigator would want to calibrate the radar in a particular field area.

Time domain reflectometry, a geophysical method which is closely related to GPR methods, can yield direct estimates of the dielectric constant of near-surface materials (Topp et al., 1980; Davis and Chudobiak, 1975). Time domain reflectometry involves inserting a wave guide into the ground and measuring the time required for an electromagnetic pulse to travel to the end of the guide, giving a measure of the pulse velocity in the soil material. Wave guides usually consist of two or more parallel rods.

The maximum measuring depth obtainable with time domain reflectometry is limited by the length of rods that can be successfully inserted into the ground. Thus TDR cannot yield accurate estimates of average dielectric constant between the surface and interfaces deeper than about one meter.

If the transmitting and receiving antennas available with a radar system can be separated from each other, wide angle reflection and refraction (WARR) sounding can be used to estimate depths to interfaces and individual layer velocities (Arcone, 1984; Davis et al., 1984; Annan and Davis, 1976; Sakayama et al., 1983; Houck, 1984; Bogorodsky et al., 1985). This method takes advantage of the fact that the squared travel time of reflections from a horizontal planar source is a linear function of the squared distance between the transmitting antenna and the receiving antenna, with the slope of this line being inversely proportional to the squared average signal velocity. This method was not employed in this study because a single antenna both transmits and receives the radar signal.

Perhaps the most straightforward calibration method is the comparison of radar data to " groundtruth" measurements of reflector depth as observed in boreholes, excavations or wells (Bogorodsky et al., 1985; Ulriksen, 1982; Haeni et al., 1987; Davis et al., 1984). In this study radar return time data are compared to measurements of water table depth in

piezometers. A primary goal of this study is to evaluate the reliability of this calibration technique when only a few observation wells or piezometers exist in the area. Subsets of the piezometers in the study area are used to determine the velocity of the radar signal in the unsaturated sands above the water table. This is done by regressing return times of reflections from the water table next to these piezometers against the observed depths to water in the piezometers. The radar velocity in the unsaturated zone is then taken to be

$$v = \frac{2}{m} \tag{9}$$

where m is the slope of the regression line. To test the accuracy of this calibration over the entire field area, radar-predicted depths at the remaining piezometers (those not used in the calibration) are compared to observed depths in those piezometers. By choosing calibrating subsets of varying size and distribution within the field area, an optimum number of calibrating piezometers can be determined. Here " optimum" means the smallest number needed to obtain an accurate calibration with an adequate estimate of the uncertainty in that calibration. The details of this analysis are presented in Chapter V.

The approach used in this study is similar to that employed by Shih et al. (1986). In a study in Florida, Shih et al. used two observation wells in a study area to calibrate the GPR and compared radar-predicted

depths based on this calibration to observed depths in 15 piezometers distributed throughout the area. They found that the absolute deviations between predicted and observed depths varied between 1 and 10 centimeters. The correlation between predicted and observed depths was 0.95.

It is important to point out that the ground surface will always appear as horizontal in the radar record. Therefore, an inverse reflection of the surface topography will be superimposed on the actual elevation variation of the subsurface interfaces. Thus, along with an estimate of radar velocity, the investigator must also obtain surface elevation data in order to derive quantitative interface elevation data from the radar record.

D. Radar Signal Attenuation

The amount of attenuation of electromagnetic energy in a given medium is a major factor governing the success of radar surveys in that medium. A measure of the amount of signal attenuation in a medium is given by the loss tangent,

$$p_e = \frac{\sigma_e}{\omega \epsilon_e} = \frac{\sigma' + \omega \epsilon' '}{\omega \epsilon' - \sigma' '} \qquad (10)$$

Both σ_e and ϵ_e are frequency dependent. However, as mentioned above, ϵ_e is approximately constant, equal to ϵ', over the frequency range of available GPR units. King and Smith (1981) show that for most dielectrics $\epsilon' '$ is essentially zero for frequencies up to about 1 MHz. Therefore, one would expect p_e to decrease as ω increases in the range of frequencies

up to at least 1 MHz. At higher frequencies, the term $\omega\epsilon''$ begins to dominate over σ' due to the increased importance of dipolar relaxation of water at higher frequencies (King and Smith, 1981; Olhoeft, 1986). In other words, more of the electromagnetic energy is dissipated in the rotation of water molecules in the medium. Therefore, as frequency increases the loss tangent is given approximately by

$$p_e \approx \frac{\epsilon''}{\epsilon'}. \tag{11}$$

The frequency at which this approximation becomes valid will vary with the material. Above this frequency, p_e should increase with increasing ϵ''. Olhoeft (1986) shows that for mixtures of varying amounts of sand and clay with water, p_e decreases in value up to a frequency of about 200 MHz. A mixture of sand and water exhibits an increase in p_e above this frequency, while mixtures of sand, clay and water show a continued decrease of p_e with increasing frequency.

The loss per unit depth is proportional to ωp_e so that, overall, attenuation increases with increasing frequency. Thus, lower frequency antennas yield better penetration than higher frequency antennas.

Equations 10 shows that the d.c. electrical conductivity, σ', of a medium has an important influence on the loss tangent. In higher conductivity media, more of the electromagnetic energy is converted to thermal energy, increasing signal attenuation (Olhoeft, 1986). Thus, highly con-

ductive clays yield much worse penetration than do resistive clay-free sands. Olhoeft (1986) shows that loss tangent increases by a factor of eight with the addition of 1.9 weight percent montmorillonite clay to a pure sand, and increases by a factor of 17 (relative to pure sand) with the addition of 4.9 weight percent clay. On this basis, the materials in the study area, primarily clean glacial outwash sand, should be an ideal medium for radar surveying.

Overall signal attenuation also increases with the number of reflectors encountered. In particular, changes in electrical properties on the scale of the signal wavelength tend to scatter the electromagnetic energy in random directions, thus decreasing the amount of energy that returns to the antenna (Olhoeft, 1986).

E. Radar Signal Resolution

A typical reflection from an interface consists of three deflections of the pulse, either one of positive polarity and two negative or vice-versa. Therefore, reflectors less than about one wavelength apart begin to become blurred on the radar record (Olhoeft, 1986; Shih et al., 1986). Thus higher frequency (shorter wavelength) antennas provide better resolution than lower frequency antennas. This factor, along with the factors influencing attenuation discussed above, means that lower frequency antennas are more appropriate for deeper surveys and higher frequency antennas are

more appropriate for surveys of soil structure and other near-surface features.

F. Strength of Reflections from the Water Table

Shih et al. (1986) discuss the factors influencing the strength of electromagnetic reflections from the water table. In general, the water table is a weaker reflector (and therefore less distinct on the graphic record) in fine materials than in coarse materials. For electromagnetic energy impinging normally on a boundary between two layers, the amplitude reflection coefficient is given by

$$r = \frac{\sqrt{\epsilon_1}-\sqrt{\epsilon_2}}{\sqrt{\epsilon_1}+\sqrt{\epsilon_2}} \qquad (12)$$

where ϵ_1 and ϵ_2 are the dielectric constants in the first and second layers, respectively (Shih et al., 1986). The square of the reflection coefficient is a measure of the reflected power at the interface (Ulriksen, 1982). Because the contrast in dielectric constant between completely dry and saturated material decreases as the grain size of the material decreases, the strength of reflections from the water table decreases with decreasing grain size. Also, Shih et al. (1986) point out that, in general, the transition between dry and saturated conditions is less abrupt in finer material than in coarser material, which further reduces the clarity of the water table in the radar record.

G. System Specifications

The radar system used in this study is a SIR System 8 marketed by Geophysical Survey Systems, Inc., and owned by the Wisconsin Department of Natural Resources. The transducer/antenna unit is the most important variable in the system. Different units operate at different center frequencies and bandwidths. The choice of which antenna to employ in a given situation should be governed by the considerations discussed in the preceding portions of this chapter. Although a 120 MHz antenna was used in the earlier (reconnaissance) portions of this project, an 80 MHz antenna was used to collect the data presented in this study. The transducer electronics mounted in the top of this unit generate a pulse 6 ns wide at a repetition frequency of 50 kHz. This pulse is fed through a bow-tie antenna, which tends to differentiate the pulse and which in turn radiates a wavelet with a center frequency of 80 MHz and 3 dB bandwidth of about 40 to 120 MHz (Horton et al., 1981). The same antenna also receives the reflected energy from subsurface interfaces. The receiver uses amplitude samples from successive returning wave forms to create an audio frequency analog (on the scale of milliseconds) of the returning signal (which is on the scale of nanoseconds).

This audio frequency analog of the returned signal is then transmitted to the system's control unit. The signal can be transferred to a tape recorder for digital recording, or printed on a graphic recorder, or both can

be done simultaneously. The graphic recorder represents deflections of the return signal from zero amplitude in shades of gray, with darkness increasing in proportion to signal amplitude. The user controls the amplitude threshold and contrast to be used for printing and also controls whether positive, negative or both positive and negative deflections of the signal are to be printed. The data recorded on digital tape can be played back to the printer, optionally with digital processing applied, at a later time.

H. Some Other Applications of GPR to Hydrogeology

Using radar profiling to obtain water table elevation data is perhaps the most obvious application of radar methods to groundwater investigations. Other projects which have included water table mapping efforts are described in Ulriksen (1982), Shih et al. (1986) and Davis et al. (1984). There are, however, other possible applications of GPR to hydrogeological problems. Radar profiling can yield information on subsurface structures which may have an important influence on groundwater flow and contaminant transport, such as stratigraphic boundaries, bedding structures and lenses of coarser or finer material. Examples of this kind of use can be found in Davis et al. (1984) and Ulriksen (1982). Ulriksen (1982) also discusses how radar methods can be used to study the location and orientation of cavities and fractures in underlying rock. GPR can also be used to profile the thickness of stream and lake sediments, thus helping to

characterize the extent of hydraulic connection between a surface water body and an underlying aquifer (Haeni et al., 1987; Davis et al., 1984).

GPR can also yield information on moisture profiles. Houck (1984) describes a method in which dielectric constant variations with depth are obtained using WARR methods as described above. Since dielectric constant is strongly correlated with soil moisture content and only weakly dependent on other soil properties (Topp et al., 1980), these variations of dielectric constant with depth can be converted to moisture profiles. However, this approach assumes that there are only step changes in moisture content at certain depths, rather than a continuous variation of moisture content. Ulriksen (1982) describes a more sophisticated method which uses frequency-dependent phenomena to obtain a more continuous moisture content profile with depth.

Investigators have also used GPR to locate subsurface sources of contamination or, in some cases, contaminant plumes. Horton et al. (1981) used GPR to locate buried barrels at several nuclear waste disposal sites. Underwood and Eales (1984) used GPR to map the extent of a buried crystalline waste mass. If a contaminant produces a sufficient alteration in the dielectric properties of the subsurface material, contaminant plumes can appear on radar records. For example, Olhoeft (1986) used GPR to locate plumes of oil and creosote products.

IV. FIELD WORK

A. Preliminary Field Work

Field work for this project began in July of 1987. For two weeks attempts were made to obtain water table profiles in the Buena Vista Groundwater Basin, the area investigated by Stoertz (1985) and Faustini (1985). A 120 MHz antenna was used for this work. Poor results were obtained in this area, possibly because the water table here is too shallow to be resolved from the reflections of the ground surface. The water table is typically about five feet deep in the central portion of the basin and the wavelength of the radar signal in the sand above the water table is about four feet. Surveys with a 500 MHz antenna in the central portion of the basin and surveys with the 120 MHz antenna over the moraines in the eastern portion of the basin (where the water table is deeper) were also unsuccessful. In both these cases, it is possible that conductive road surface materials contributed to the poor quality of the results. Another possible explanation for the poor results is that the predominant soil types in the basin have surface layers of muck which obscure reflections from the water table. The influence of soil type on signal quality is discussed in detail in section C of this chapter.

At the end of this two week period, surveys were made in the area of the northern boundary of the Buena Vista Groundwater Basin, formed

by a water table divide. North of this divide groundwater flows generally northward to the Wisconsin River. GPR surveys yielded fairly clear water table profiles throughout much of this area. Because of the success of these surveys and because of the abundance of existing piezometers in this area, it was chosen as the area of detailed study for this project. For a description of the field area, see Chapter II.

During October of 1987, an attempt was made to carry out detailed GPR surveys and collect water level measurements in the field area. However, rain and technical difficulties with the radar system allowed only patchy data to be collected during these two weeks. A detailed survey of road surface elevation around one block in the field area was performed during this time. This survey has been used to evaluate the uncertainty in road surface elevations obtained from interpolating between data points shown on topographic maps for the area.

B. Detailed Surveys in the Field Area

Systematic radar surveys along roads in the field area were obtained during the first week of November, 1987. Water levels in most of the piezometers in the field area were also measured during this week. Additional water level measurements were provided by Kraft (personal communication), who had made water level measurements throughout October.

Figure 6 shows the distribution of data points in the field area. Radar surveys were performed along roads in the study area by towing the antenna behind an automobile containing the control unit, tape recorder and graphic recorder. A vertical mark was printed on the radar record every twentieth of a mile, as estimated from the automobile odometer. Water table return times were later picked off the record at each of these marked points. Thus the GPR data points shown on Figure 6 are at intervals of one-twentieth of a mile. There are 280 GPR data points. Of course, the actual record is continuous, so a finer or coarser level of discretization could have been chosen. Examination of the radar records reveals that this level of discretization is fine enough to characterize any real variations in water table depth. Most of the variation at smaller scales than this is probably due to small-scale elevation changes of the road surface, rotations of the antenna as it rolls along the road and other apparently random effects. Two or more surveys were carried out along most of the roads, so that repeat observations were obtained at most of the GPR data points shown in Figure 6.

C. Influence of Soil Type

There appears to be a strong correlation between the quality of the radar signal and soil type in the field area. Otter and Fiala (1978) show two dominant soil types in the field area. A swath of Friendship loamy

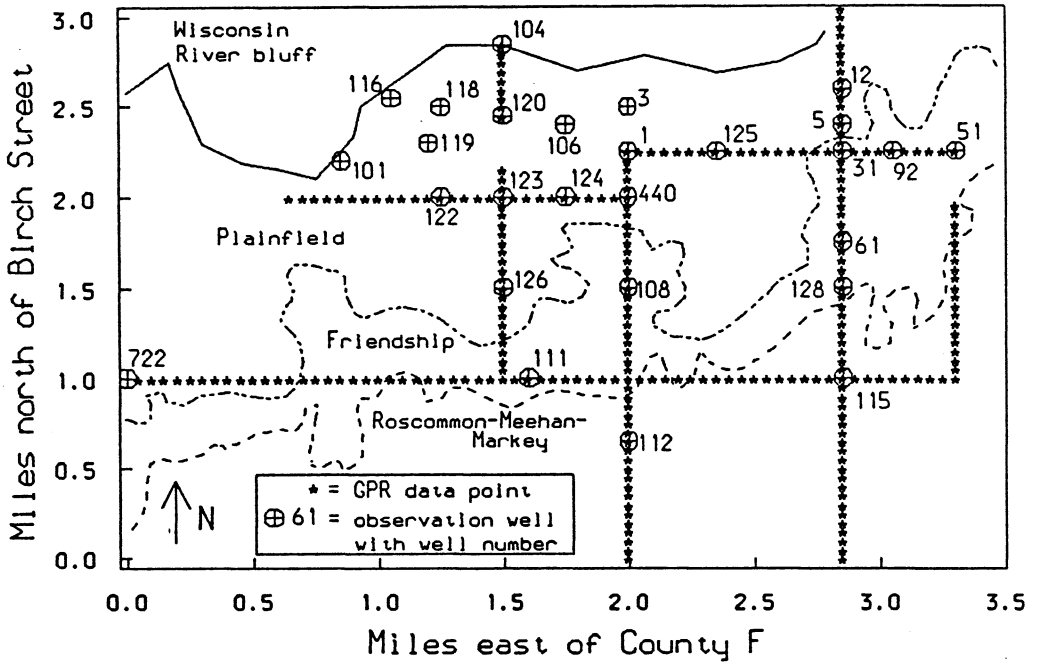

Figure 6. Distribution of data points in the field area with soil type boundaries shown by dashed lines. Birch Street and County Highway F are shown on Fig. 2.

sand runs approximately southwest-northeast, occupying perhaps a quarter of the field area. North of this swath, the Plainfield loamy sand predominates and south of it a complex intermingling of soils of the Roscommon-Meehan-Markey association occurs.

Figures 7 and 8 show radar records obtained over Plainfield loamy sand soils and Friendship loamy sand soils, respectively. The distinct difference in the clarity of the profile between these two soils is consistent throughout the field area, with changes in quality coinciding almost exactly with the soil boundaries shown in Otter and Fiala (1978). It is difficult to distinguish the water table in much of the record obtained over the Friendship soils. The descriptions of these soils in Otter and Fiala are almost identical, except that the upper loamy sand portion of the Friendship soils is slightly thicker than the upper loamy sand portion of the Plainfield soils. The Friendship soils are described as having an upper layer of loamy sand from 0 to 7 inches and a lower layer of loamy sand from 7 to 19 inches below the land surface. The Plainfield soils have an upper loamy layer from 0 to 5 inches and a light loamy sand from 5 to 14 inches below the land surface. It seems unlikely that such a slight variation should cause such a dramatic difference in signal quality, especially since the water table in this area is below these loamy sand horizons. However, the correlation between soil type and signal quality is quite strong. Perhaps some other subsurface variation, such as the occurrence

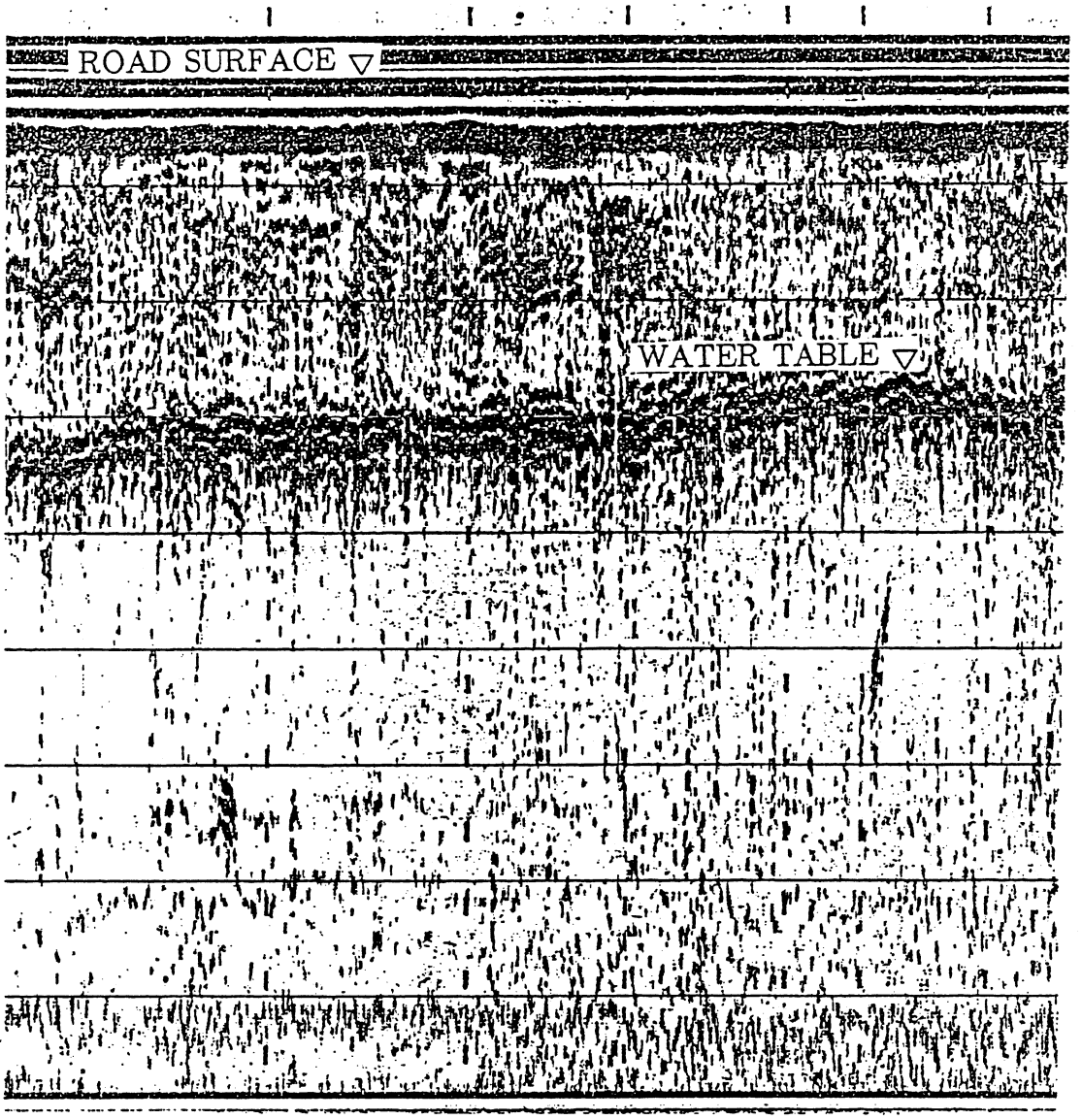

Figure 7. Typical radar record from a survey over Plainfield loamy sand soil. The vertical marks at the top of the record are at intervals of one-twentieth of a mile. The vertical scale is 17.2 ns/cm.

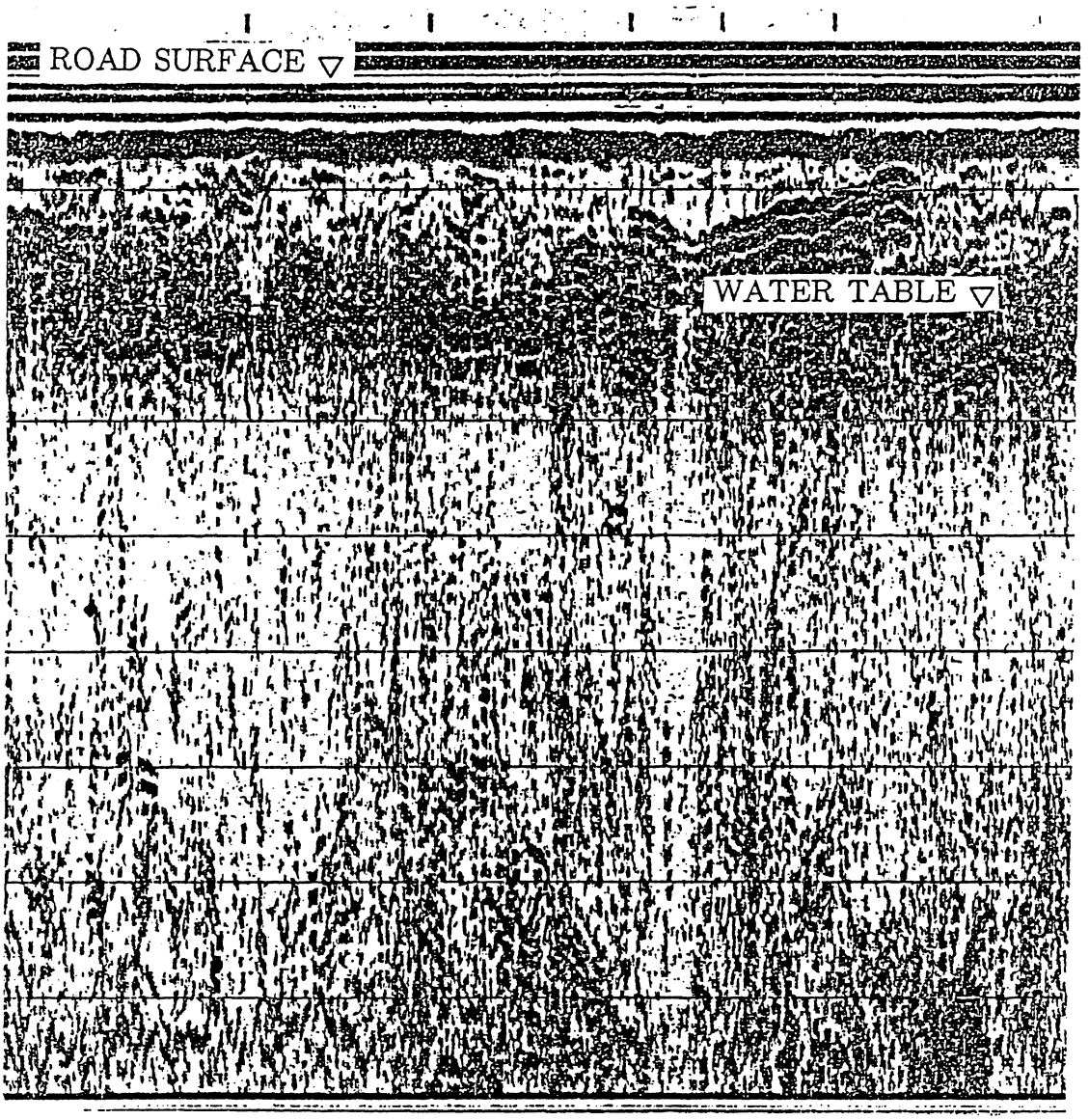

Figure 8. Typical radar record from a survey over Friendship loamy sand soil. The vertical marks at the top of the record are at intervals of one-twentieth of a mile. The vertical scale is 17.2 ns/cm.

of finer materials at depths of a few feet or more under areas of Friendship soils, not only influences the quality of the radar signal, but also influences the development of the overlying soils by causing variations in drainage conditions.

The radar profiles obtained in soils of the Roscommon-Meehan-Markey series contain adequately clear water table reflections, although they are not as clear as those from profiles over Plainfield soils. The Roscommon and Markey both have surface layers of muck, about nine inches thick in Roscommon soils and 16 to 51 inches thick in Markey soils (Otter and Fiala, 1978). One would not expect very good radar profiles in such soils. However, the Meehan loamy sand apparently underlies most of the surveyed roads in the southern half of the study area. The Roscommon and Markey soils predominate farther to the south, in the central portion of the Buena Vista Groundwater Basin. This is perhaps the best explanation for the fact that radar records from surveys in the basin were in general quite cluttered.

V. EVALUATION OF RADAR PREDICTION ACCURACY

A. Introduction

As discussed in the previous chapter, during the first week of November, 1987, GPR surveys of water table depth were performed along county roads in the field area. Water levels in piezometers in the field area were also measured during the same week and during the last two weeks of October. For the following analysis, the measured depths were corrected for the difference in elevation between the measuring point of the piezometer and the road surface next to the piezometer, since the radar is measuring the depth below the road. In the following discussion, these corrected depths will be called the observed depths at the wells. In this chapter, these data are used to evaluate the predictive accuracy of the radar calibrating model given in equations 8 and 9.

Four methods of evaluation are used: 1) Water table return times at all 21 calibrating wells are regressed against observed water depths in those wells. This regression model is analyzed with particular attention to the influence of soil type on model results. 2) Radar signal velocities calculated at individual wells are mapped to determine whether they exhibit any trend in space. This is an important factor in the study, since the main source of uncertainty in calibration results is the influence of lateral variation of signal velocity in the subsurface. These results are also used

to analyze possible dependence on soil type. 3) Subsets of wells are actually used to calibrate the radar and this calibration is used to predict water table depths throughout the field area. Predictions at the remaining observation wells are compared to observed depths at these wells and the correlation, bias, root mean squared deviation and maximum deviation between observed and predicted results are calculated. This analysis essentially simulates and evaluates an actual reconnaissance study, where only a few calibrating wells or piezometers exist in an area. 4) Radar-predicted water table depths for each calibrating subset of wells are subtracted from surface elevations at the radar data points and the resulting data are used to produce maps of water table elevation. These maps are compared to a map produced using data from all 27 observation wells in the study area. For two of the calibrating subsets, the actual maps are shown. Numerical comparisons are tabulated for all subsets chosen.

All regression techniques discussed in this chapter are described in Draper and Smith (1981). The data analysis was performed on the data analysis and graphics system, S (Becker and Chambers, 1984).

B. Analysis of Regression With All Wells

Figure 9 shows the GPR return time data plotted against observed depths at all 21 potential calibrating wells. Note that there are replicate return time values at most of the wells, giving a total of 36 data points.

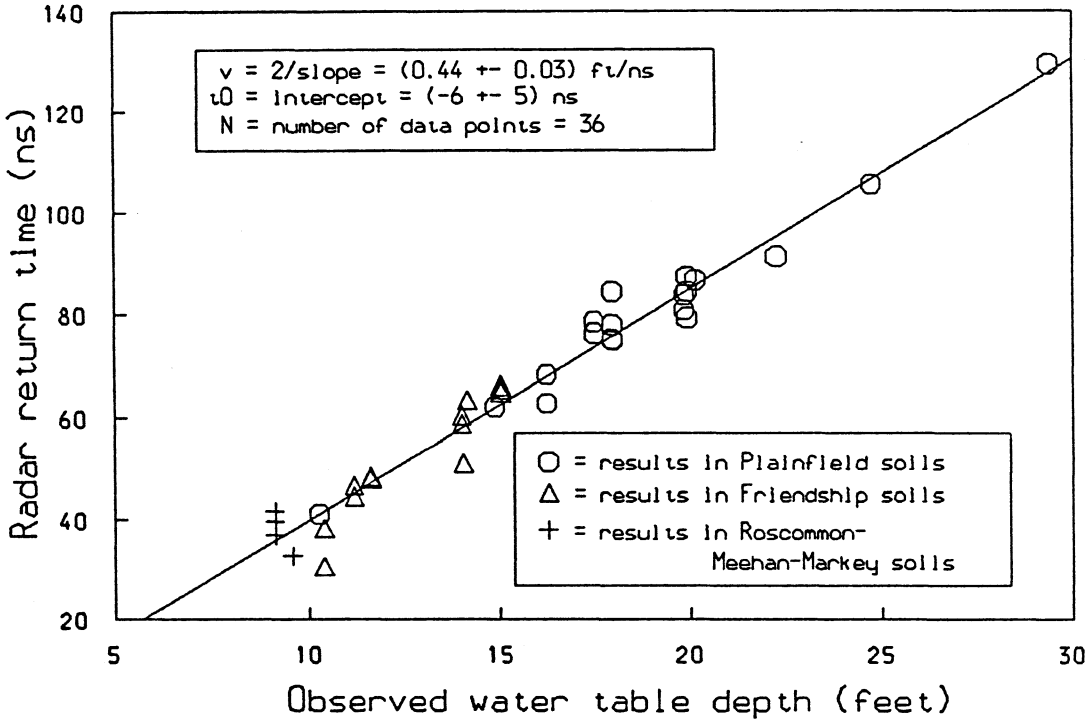

Figure 9. Regression of radar return time versus water table depth for all 21 wells.

Results from wells in different soil type regions are plotted with different symbols. A straight line has been fit to the data using linear least squares regression. The regression model is given by

$$t_r = \beta_0 + \beta_1 D + \epsilon \qquad (13)$$

where t_r is the observed water table return time, β_0 is the intercept term, β_1 is the slope of the line, D is the observed depth of water at a well and ϵ is a term representing random variation in the data. Note that a non-zero intercept term, β_0, has been included in this regression, making the proposed model slightly more complicated than that given by equation 8. When the above model is applied to a particular set of data, the resulting line yields estimates of the model parameters β_0 and β_1. The fitted slope, m, estimates β_1. The calibrated velocity is taken as $\frac{2}{m}$, as shown in equation 9.

In the following analysis, the fitted intercept will be called the return time correction factor, labelled t_0. t_0 is an estimate of the theoretical parameter, β_0. The primary reason for including an intercept term is to account for a possible difference in radar signal velocity between the sediments above the range of depths over which the water table varies and the sediments in that depth range. A simplified model of the subsurface materials will help to clarify the meaning of this intercept term. The water table in the study area varies from 10.3 to about 30 feet in depth.

If it is assumed that the sediments in this depth range can be characterized exactly by a constant radar signal velocity, v_a, when they are above the water table, and that the sediments from 0 to 10 feet in depth can be characterized by a radar signal velocity given by $v_a + \delta v$, then the velocity given by the above calibration technique will be exactly equal to v_a (assuming that there is no error in the measurements of radar signal return time and water table depth). The return time correction factor in this simplified case will be given by

$$t_0 = -\frac{2D_0\delta v}{v_a(v_a+\delta v)} \tag{14}$$

where D_0 is the minimum depth of the water table, here 10.3 feet. If δv is sufficiently small compared to v_a, then t_0 is approximately directly proportional to δv and inversely proportional to $v_a{}^2$.

Table 1 is an analysis of variance table for the resulting regression. Replicate return time observations at certain wells are used to determine the pure error sum of squares. The pure error mean square, given by the pure error sum of squares divided by its degrees of freedom, n_{pe}, is taken as an estimate of the inherent random variation in the data. The lack of fit sum of squares is the difference between the total variation about the fitted line (the residual sum of squares) and the pure error sum of squares. The lack of fit sum of squares divided by its degrees of freedom, n_{lf}, gives the lack of fit mean square. Under the assumption that there is no

Table 1. Analysis-of-variance table for regression of water table return time versus observed water table depth at all 21 calibrating wells. Results shown are the sum of squares (SS) due to a given source, the associated degrees of freedom (df) and the mean square (MS) due to that source, given by SS/df. The first F value is the ratio of the mean square due to regression to the mean squared residual and the second is the ratio of the mean square due to lack of fit to the mean square due to pure error.

source	SS	df	MS	F
regression	16387.13	1	16387.1	1059.3
residual	525.9861	34	1.55	
lack of fit	380.2757	19	20.01	2.06
pure error	145.7104	15	9.71	
total,corrected	16913.11	35		

significant lack of fit in the model, then the lack of fit mean square should also estimate the random variation in the data and the ratio of the lack of fit mean square to the pure error mean square should follow an F distribution with n_{lf} degrees of freedom for the numerator and n_{pe} degrees of freedom for the denominator. This assumption means that the model adequately describes most of the non-random variation in the data. If the lack of fit mean square is significantly larger than the pure error mean square, this is taken as an indication that the proposed model does not adequately account for the non-random variation in the data and that a better model should be proposed. The test for lack of fit is performed by comparing the observed ratio of lack of fit mean square to pure error mean square to the 95% significance level of an F distribution with the proper degrees of freedom. If the observed ratio is larger than this theoretical F value then we can reject the hypothesis that there is no lack of fit at the 95% confidence level.

As Table 1 shows, the observed lack of fit F value is 2.06. The 95% significance level of an F distribution with 19 degrees of freedom for the numerator and 15 for the denominator is 2.34. Since the observed F value is smaller than this theoretical F value, then we cannot reject the hypothesis that there is no lack of fit in the model. In other words, the model is said to show no statistically significant lack of fit (at the 95% significance level).

Having determined that there is no statistically significant lack of fit in the model, we can perform an F-test for the significance of the regression by comparing the variation accounted for by the fitted line to the total variation about the fitted line. The sum of squares due to regression is the total variation explained by the fitted slope. The mean square due to regression is the same as the sum of squares due to regression, since there is only one degree of freedom associated with the fitted slope. The observed F value for the significance of the regression is given by the ratio of the mean square due to regression and the mean squared residual. Since we are fitting two parameters, slope and intercept, the degrees of freedom for the mean squared residual is given by $n-2$, where n is the number of data points. Under the hypothesis that the " true" slope of the line, β_1, is zero, this ratio follows an F distribution with 1 and $n-2$ degrees of freedom. As shown in Table 1, the observed F of regression is 1059, which is much larger than 4.13, the 95% confidence level for an F distribution with 1 and 34 degrees of freedom. Therefore the regression is very significant.

The tests for lack of fit and significance of regression are based on the assumption that the residuals from the regression are normally distributed with mean zero. Ideally, these residuals should also show no dependence on the observed water table depth, which is the predictor variable in the this model. Figure 10 shows the residuals plotted against observed water table depth, with results in different soil types represented by

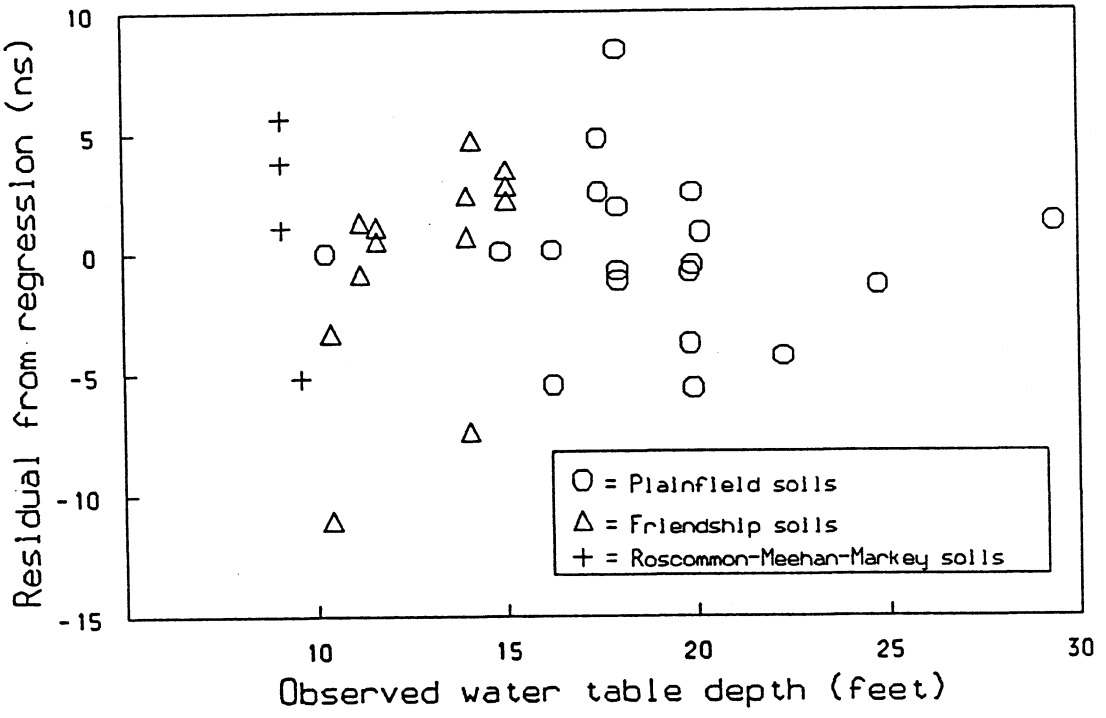

Figure 10. Residuals from regression of return time versus depth for all 21 wells.

different symbols. The residuals appear to be fairly uniformly distributed over all depths, as one would hope. The fact that there are no replicate values for the three greatest depths (at wells 1, 120 and 104) probably explains the apparent decrease in variance of the residuals at greater depths.

Figure 11 shows a normal plot of the residuals from the regression, again with residuals from different soil types represented by different symbols. In this plot the quantiles of a standard normal corresponding to the Blom plotting positions for the ranked residuals are plotted on the vertical axis and the residuals are plotted on the horizontal axis. If the residuals actually represent samples from a normal distribution, the resulting plotted points should fall approximately on a straight line. In Figure 11 the bulk of the data does closely follow a straight line. The residuals from the three different soil types all seem to exhibit similar behavior, indicating that there is no strong reason to doubt that they come from the same distribution. However, the distribution of residuals seems to be somewhat heavier in the negative tail than would be expected of a random sample from a normal distribution. Some deviation from the line is typical at the extremes of the data, so it is difficult to determine how significant this deviation from normality actually is. For the purposes of this discussion, the residuals will be considered normal enough to justify the lack of fit and significance of regression tests made above.

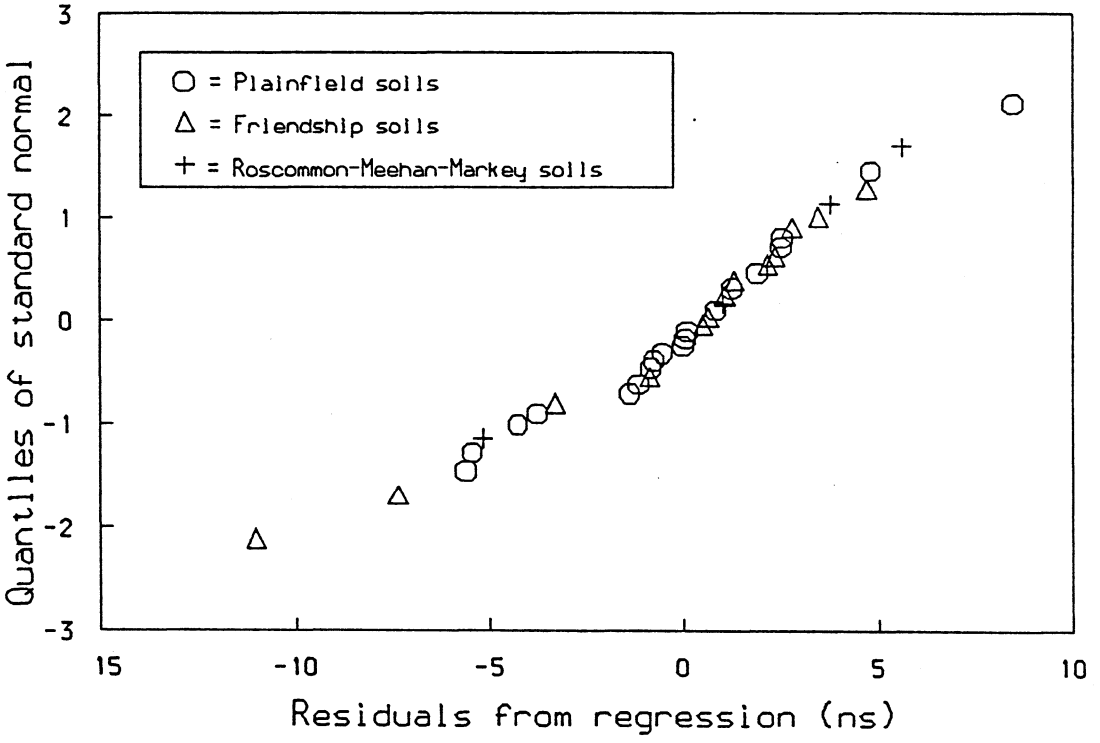

Figure 11. Normal plot of residuals from regression of return time versus depth for all 21 wells.

To test whether soil type has a significant influence on regression results, a dummy variable, Z, representing soil type is introduced into the regression equation. This dummy variable is given a value of 0 for all wells in Plainfield soils and a value of 1 for all wells in Friendship soils. Since a total of only four data values were obtained from the two wells in soils of the Roscommon-Meehan-Markey complex, these data have been left out of this analysis. Including a third soil type in the analysis would have required introducing a second dummy variable, an action which is probably not justified, since there are so few data points in these soils. The regression model, with the dummy variable included, is given by

$$t_r = \beta_0 + \beta_1 D + \gamma_0 Z + \gamma_1 ZD + \epsilon \qquad (15)$$

Thus, the model is free to fit both a different slope and a different intercept to the results in each soil type. The significance of the contribution of the Z terms to the model results is again determined by an F-test, comparing the amount of variance accounted for by the introduction of this variable to the mean squared residual from the full model (the one including the Z terms). Since there are two parameters associated with Z and there are 28 residual degrees of freedom for the full model, the appropriate F distribution is one with 2 degrees of freedom for the numerator and 28 for the denominator. The observed ratio of the mean variance explained by the Z terms to the mean squared residual from the full model is 2.37. This is less than 3.34, the 95% significance level for the appropriate F

distribution. It is, in fact, less than the 90% significance level, 2.50. Therefore it is concluded that the soil type does not have a statistically significant influence on the regression results.

The above tests indicate that there is no strong reason to doubt the adequacy of the regression model represented by equation 13. The estimate of radar signal velocity obtained from this regression, with a 95% confidence interval, is $0.44 \pm 0.03 \frac{ft}{ns}$. The 95% confidence interval is estimated from first order analysis: since v is inversely proportional to the fitted slope, m, the coefficient of variation of v (the ratio of the standard error in v to the estimate of v) is approximately the same as the coefficient of variation of m, which can be determined from the regression results. Since the residual degrees of freedom for a fitting a straight line (a two-parameter model) to n data points is $n-2$, the standard error in v is multiplied by the 2.5% exceedance value for a t distribution with 34 degrees of freedom to obtain a 95% confidence interval for v. The 95% confidence interval for t_0 is obtained by multiplying the standard error of the intercept obtained from the regression by the same t value. This yields an estimate for t_0 of -6 ± 5 ns.

The estimated velocity corresponds to a dielectric constant of 5.2, which is in the expected range for dry sand (4 to 6). Using equation 14 and assuming $v_a = 0.44 \frac{ft}{ns}$ and $D_0 = 10.3\ ft$, a value of $t_0 = -6$ ns

corresponds to a value of $\delta v = 0.06 \frac{ft}{ns}$. Thus, assuming that the simplified model implicit in equation 14 approximately describes the materials in the field area, there is only a slight difference, if any, between the radar signal velocity in the sediments in the depth range over which the water table varies and those above that range.

C. Spatial Distribution of Signal Velocity

Figure 12 shows a map of velocities calculated at individual wells in hundredths of a foot per nanosecond. These velocities are calculated by dividing twice the observed depth of water at each observation well by the average water table return time at that well (eqn. 8). It is important to point out that these velocity values are larger than that calculated from the above regression because the non-zero intercept term in the regression allows for a lower velocity value. These calculations assume that t_0 is equal to zero.

The velocity results show no obvious trend in space. The soil type boundaries are also included on the map. It appears as if the velocities calculated in areas with Friendship soils exhibit somewhat more variation than those calculated in Plainfield soils. Figure 13 is a comparative plot of the distributions of velocity values calculated in each soil type. Each point plotted represents represents a velocity calculated at a single well, so that each stack of points is essentially a vertical histogram of signal

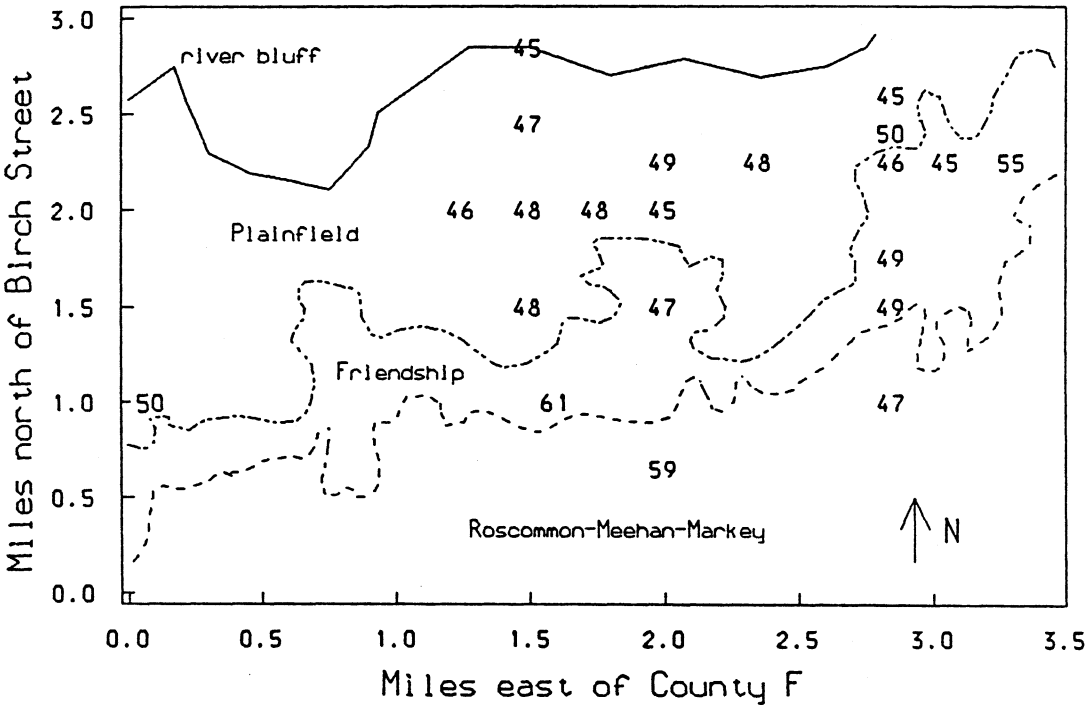

Figure 12. Radar velocities in 10E-2 ft/ns at individual wells, mapped with soil type.

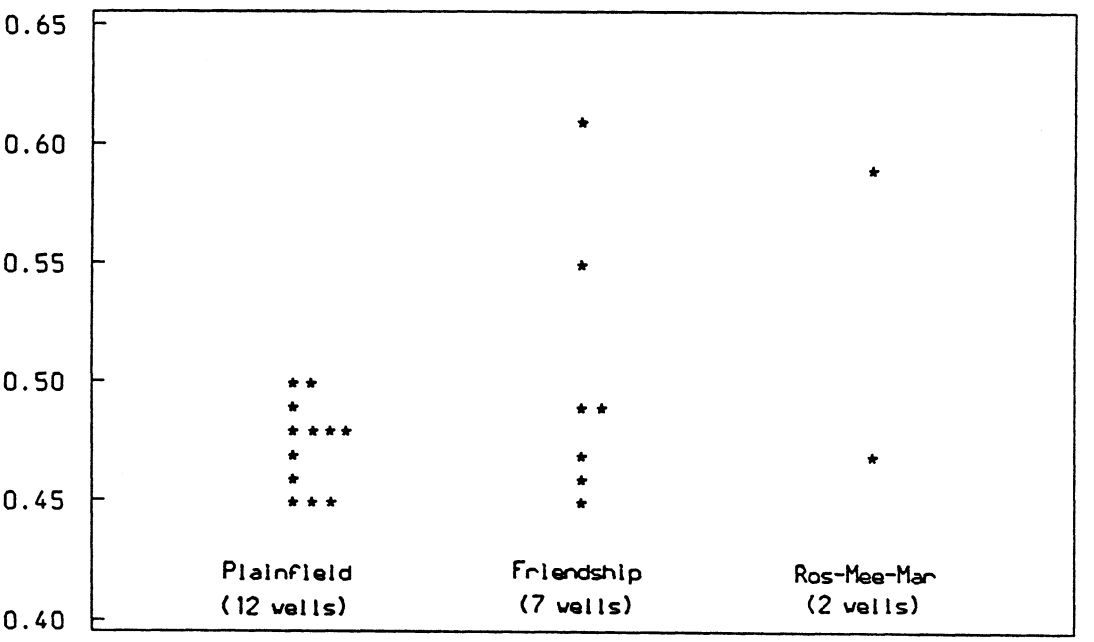

Figure 13. Radar signal velocities in ft/ns calculated at wells in Plainfield, Friendship and Roscommon-Meehan-Markey (Ros-Mee-Mar) soils.

velocities in a given soil type. Because only seven velocity values for Friendship soils are available, it is difficult to determine whether the two higher values calculated (0.55 and 0.61 $\frac{ft}{ns}$) are outliers or not. If these two values are considered to be representative of the distribution of velocities in Friendship soils then one would conclude that this distribution exhibits more variation and is skewed toward higher values than the distribution of velocities in Plainfield soils. A higher variance in results in Friendship soils might be expected considering the poor signal quality of radar records in Friendship soils. If these two values are considered to be outliers, then one would conclude that there is no significant difference between the velocities calculated in areas of Friendship and Plainfield soils.

D. Sample Calibrations and Water Table Depth Predictions

For the results presented in this section the following procedure was used to calibrate the radar and predict water table depths:

1) Different subsets of observation wells were chosen and, for each subset, water table return times were regressed against observed water table depths, as in section B of this chapter. The calibrated velocity, v, the return time correction factor, t_0, and the 95% confidence intervals for these estimates were obtained from the regression results, also as described in section B. If the subset consisted of only one well, the velocity was determined by dividing twice the observed depth at the well by the mean

return time at that well, as in section C of this chapter. Thus, no return time correction factor was included and no estimate of uncertainty was obtained if the calibrating set consisted of one well. If the subset consisted of two wells, the mean return times at the two wells and the observed depths were used to fit (exactly) a straight line with a non-zero intercept term included. Again, no estimates of uncertainty were obtained in this case.

2) At each GPR data point, a water table depth value was determined from the mean return time, $t_{r\,m}$, at that point and the above calibration. The predicted depth is given by

$$D_{pr} = \frac{v\,(t_{r\,m} - t_0)}{2}. \qquad (16)$$

3) The accuracy of the predicted depths was evaluated by comparing the depths predicted at wells which were not included in the calibrating set to the observed depths at those wells. In particular, the correlation, root mean squared deviation, bias and maximum deviation between the predicted and observed results were calculated. The bias was estimated as the mean difference between the predicted and observed depths. The root mean squared deviation is an estimate of the expected error in depth prediction results and is perhaps the best overall measure of prediction accuracy.

Table 2 shows the results of the above analysis for various sets of

Table 2. Results of radar calibration and depth prediction accuracy at remaining wells for various sets of calibrating wells; calibrated velocity (v) and return time correction factor (t_0) are shown with 95% confidence intervals, if available; prediction accuracy results are correlation (cor), root mean squared deviation (rmsd), bias and maximum deviation (maxd) between radar-predicted and observed water table depths.

	GPR calibration		Depth prediction accuracy			
well set	$v(\frac{ft}{ns})$	t_0(ns)	cor	rmsd (ft)	bias (ft)	maxd (ft)
115	0.47	0	0.991	1.00	-0.46	-2.39
440	0.45	0	0.991	1.23	-0.94	-2.63
125	0.48	0	0.990	0.99	-0.01	-2.18
108	0.47	0	0.991	0.98	-0.31	-2.32
440, 722	0.40	−10	0.990	1.02	-0.65	-1.84
115, 125	0.49	2	0.991	1.15	-0.07	-2.46
440, 722, 51	0.38 ± 0.19	−17 ± 43	0.992	0.96	-0.27	-1.78
115, 125, 122	0.47 ± 0.07	0 ± 9	0.990	1.05	-0.40	-2.38
440, 722, 51, 115, 125	0.45 ± 0.09	−4 ± 13	0.992	0.79	-0.33	-1.95
440, 722, 51, 115, 125, 112, 104	0.43 ± 0.05	−6 ± 9	0.987	0.71	-0.23	-1.65
all wells in Plainfield soils	0.44 ± 0.04	−5 ± 9	0.929	1.01	-0.25	-1.71
all wells in Friendship soils	0.34 ± 0.08	−23 ± 18	0.995	1.70	-1.10	-3.33
all 21 wells	0.44 ± 0.03	−6 ± 5	–	–	–	–

wells. The first four calibrating sets consist of individual wells. Well 115 is in the southeast part of the study area and is in an area of Meehan soils; 440 and 125 are both in the central part of the area and are in Plainfield soils and 108 is in the central part of the area in Friendship soils. It is interesting that the calibrations against wells 440 and 125 give the most extreme results of this group of calibrations. The calibration against well 440 yields the lowest velocity, the largest root mean squared deviation and the largest bias and maximum deviation. The calibration against well 125 yields the highest velocity and smallest bias and maximum deviation. The results of the calibrations against well 115 and against well 108 are very similar. These observations indicate that the variation among results is fairly random and is not strongly influenced by the location of the calibrating well or the soil type at that well. The results shown for calibrations against all wells in Plainfield soils and all wells in Friendship soils seem to contradict this hypothesis, since the prediction results are fairly different between these two groups. However, these two sets of results can be considered a worst-case comparison, since the calibration against all the wells in Friendship soils are being used to predict depths mainly at wells in the area of Plainfield soils, and vice-versa.

The next six lines show calibration and depth prediction accuracy results for sets of two, three, five and seven wells. Repeat observations at one or two wells could provide three or more data points for the

calibration and thus provide enough degrees of freedom to obtain an estimate of the pure error component of the uncertainty in the calibration parameters, v and t_0. However, the most important source of variation in the data to identify, beyond that accounted for by the model, would be lateral variation in the radar signal velocity. Therefore, at least three wells are needed in an area to obtain an adequate estimate of the uncertainty in the calibration parameters. Alternatively, one could assume that t_0 is equal to zero (constraining the regression line to pass through the origin). Given this assumption, two wells are the minimum number needed to obtain an estimate of the uncertainty in v. An increased number of calibrating wells would increase the degrees of freedom on which estimates of uncertainty are determined and therefore increase an investigator's confidence in these estimates.

As shown in Table 2, most calibrating well sets yield a correlation of about 0.99 and a root mean squared deviation of about 1 foot between radar-predicted and observed water table depths. One would expect that depth prediction accuracy would tend to increase with increasing number of calibrating wells, since larger sets are less likely to be dominated by results at wells where the radar signal velocity is anomalously high or low. However, especially for small sets of calibrating wells, depth prediction accuracy does not necessarily improve with increasing number of calibrating wells, since wells that are fairly representative of average conditions

may be combined with wells that are less representative. For instance, the calibration against well 125 yields slightly lower root mean squared deviation and bias than the calibration against wells 115, 125 and 122. Nevertheless, it should be noted that although calibration against a single well can give reasonable depth prediction accuracy results, such a calibration does not give the investigator any means of assessing the validity of these results.

The most consistent result shown in Table 2 is that all the biases and maximum deviations are negative, meaning that radar-predicted depths are consistently low compared to the observed depths. The reasons for this are unknown. One possible source of bias is the fact that the original regression equation (which gives return time as a function of observed depth) is inverted to predict a depth corresponding to a given return time. The inverted regression equation would not necessarily yield an unbiased estimate of depth. Despite this problem, a regression of return time versus observed water table depth has been used to calibrate the radar for two reasons: 1) Classical regression theory is based on the assumption that the predictor (independent) variables in a postulated model are not subject to error (Draper and Smith, 1981). In this study, measured depths of water in wells are subject to considerably less relative error than the water table return times read off the GPR records. Therefore, it seems reasonable to make D the predictor variable in the

regression equation used to calibrate the radar. 2) There are repeat observations of water table return time at most wells. These repeat values can be used to determine lack of fit in a regression model which gives t_r as a function of D. However, a set of data which contains repeat observations of t_r for a given value of D would not necessarily contain repeat observations of D for a given value of t_r. Therefore, this data would not necessarily yield information on the lack of fit in a regression model postulating D as a function of t_r. (It is fairly likely, however, that the data would contain " approximate repeat" values of D, that is observations of D corresponding to two or more very similar values of return time. This information could be used to determine model lack of fit once the investigator decided, for a particular set of data, how close return time values should be to classify the corresponding depth values as approximate repeats (Draper and Smith, 1981).)

To investigate the magnitude of bias introduced by inverting the calibrating model, an alternative method of calibration was tested: For a given set of wells, observed water table depths were regressed against water table return times to give an equation describing D as a linear function of t_r. (A non-zero intercept term was included in this equation, as in the original calibrating model.) The fitted equation was then used directly to predict water table depths from water table return times. This alterna-

tive calibration procedure was used for several of the sets of calibrating wells shown in Table 2. The depth prediction results based on this calibration showed no substantial improvement and were in some cases worse. For example, for the calibrating set consisting of wells 440, 722 and 51, the alternative calibration yielded a root mean squared deviation of 1.22 feet, a bias of -0.31 foot and a maximum deviation of -2.57 feet between radar-predicted and observed depths. For the calibrating set consisting of wells 115, 125 and 122, the alternative calibration yielded prediction results with a root mean squared deviation of 1.03 feet, a bias of -0.41 foot and a maximum deviation of -2.34 feet.

E. Water Table Elevation Prediction Results

To produce a map of water table elevation from radar-predicted water table depths, these depths must first be subtracted from the road surface elevation at each GPR data point. For this study, road surface elevations at the data points were obtained from linear interpolation between elevation data on topographic maps for the study area. Comparison between interpolated road surface elevations and elevations obtained in a detailed survey around the block defined by Hayes Avenue, Meehan Drive, Monroe Avenue and Prairie Drive (Figure 2) in the central part of the study area indicates that the expected error in interpolated elevations is about one foot. The detailed road surface survey also indi-

cated that the road surface is fairly noisy; dips and rises several feet in amplitude and with horizontal scales of 50 to several hundred feet are superimposed on very gentle overall slopes of two to three feet per mile. This noise combines with that in the radar-predicted depths to produce a great deal of random variation in the radar-predicted water table elevations.

These noisy data must be both smoothed and interpolated to a regular grid of points to produce a water table map and to produce input for the mass balance model used in this study to calculate recharge rates. In this study, a single procedure is used to produce a smooth water table surface from the GPR-predicted elevations: a cubic polynomial in the horizontal coordinates is fit to the radar data by linear least squares regression and the resulting equation is then used to calculate water table elevations at all points in a regular grid superimposed on the study area. This regular array of data can then be contoured to produce a water table map. The same grid is also used as the nodal mesh in the mass balance model, so that the results of this interpolation are used directly as input to the model. The spacing between nodes in the grid is one-tenth of a mile in both the east-west and north-south directions. The study area is 3.3 miles on a side, so that the entire grid of interpolating points forms a 34 by 34 array. However, interpolated elevations are not extrapolated outside the polygon formed by the radar survey data. Grid points outside this

polygon are not used when contouring to produce maps and are ignored in the mass balance model.

In this section, water table maps produced using the calibrating well sets shown in Table 2 are compared to the water table map produced from linear interpolation between water table elevations at all 27 observation wells in the field area, including the six which are not potential calibrating wells, specifically numbers 101, 116, 118, 119, 106 and 3 (Figures 2,6). In the following discussion, the surface produced by linear interpolation among the wells, shown in Figure 14, will be called the interpolated water table and the surfaces produced by fitting cubic polynomials to GPR-predicted water table elevations will be called radar-predicted water tables. This terminology is used simply for convenience; the process used to produce the radar-predicted water tables, described above, is also a kind of interpolation technique. The same grid is used for the interpolated water table as is used for the radar-predicted water tables, so that numerical comparisons between the maps can be made.

It should be noted that the interpolated water table is taken as a reference value for the radar-predicted water tables primarily because it is produced by more conventional and simpler means and its relationship to observed water levels is more direct than that of the radar-predicted water tables. Whether it is a more accurate representation of the true water table is an open question. The accuracy of an interpolated water table

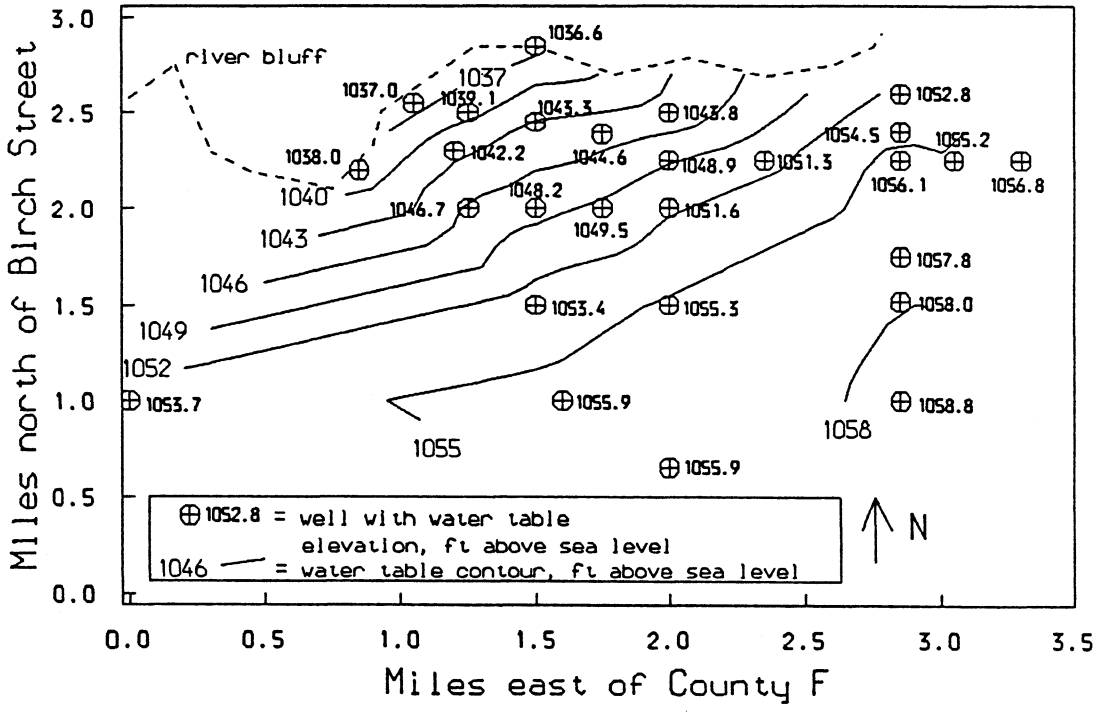

Figure 14. Water table map from linear interpolation of observation well data, fall 1987.

will depend on the quality and density of water table elevation data, the complexity of the actual water table and the interpolation technique employed.

Figure 14 shows the interpolated water table sloping toward the river bluff, with the slope increasing nearer the river. The bend in the 1055 contour line is probably a weak hint of the groundwater divide which should run approximately east-west across the southern portion of the area. The position of the divide as shown in Figure 2 is based on maps prepared by Faustini (1985). South of this divide the water table would be expected to slope southward toward Drainage Ditch Number 1, which runs along the southern edge of the study area east of Monroe Avenue and angles to the southwest west of Monroe Avenue. However, the well data do not extend far enough south to confirm the position (or existence) of this divide.

Figure 15 is the water table map produced from fitting a cubic polynomial in the horizontal coordinates to the 280 radar-predicted elevations based on the calibration against well 440. A map of differences in elevation between this surface and the interpolated water table, Figure 16, shows that the radar-predicted water table is generally higher than the interpolated water table. The radar-predicted water table is consistently higher toward the south of the study area. The differences are less consistent toward the north, although they are still generally positive. Figure

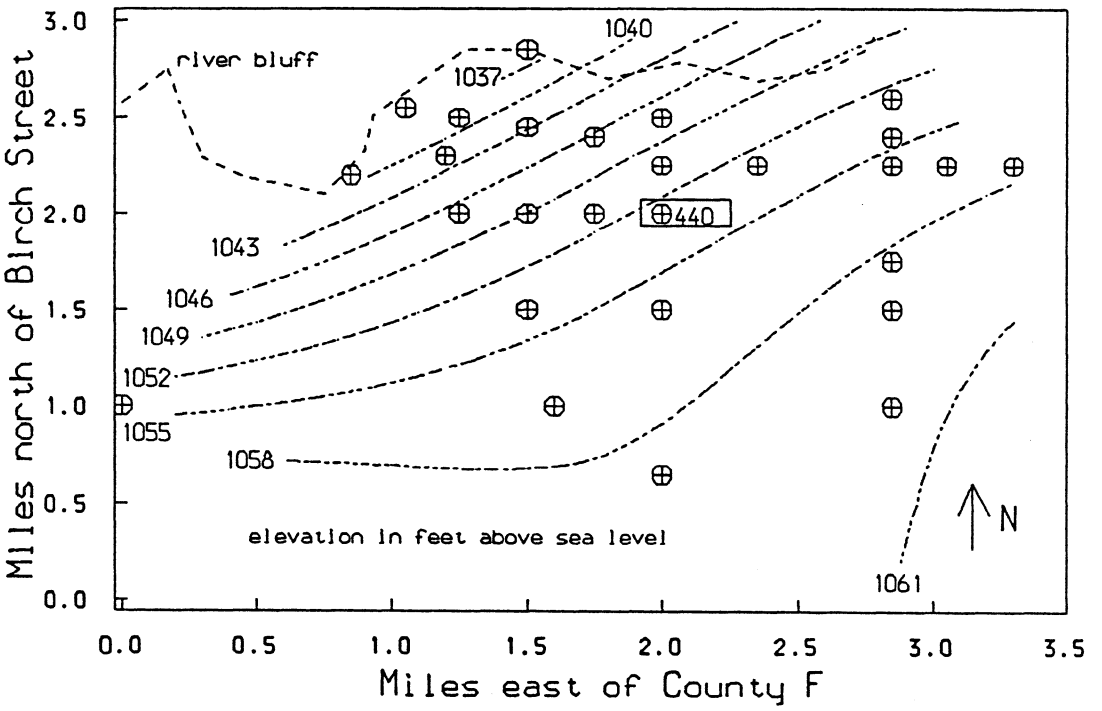

Figure 15. Water table map from cubic fit to GPR data calibrated against well 440.

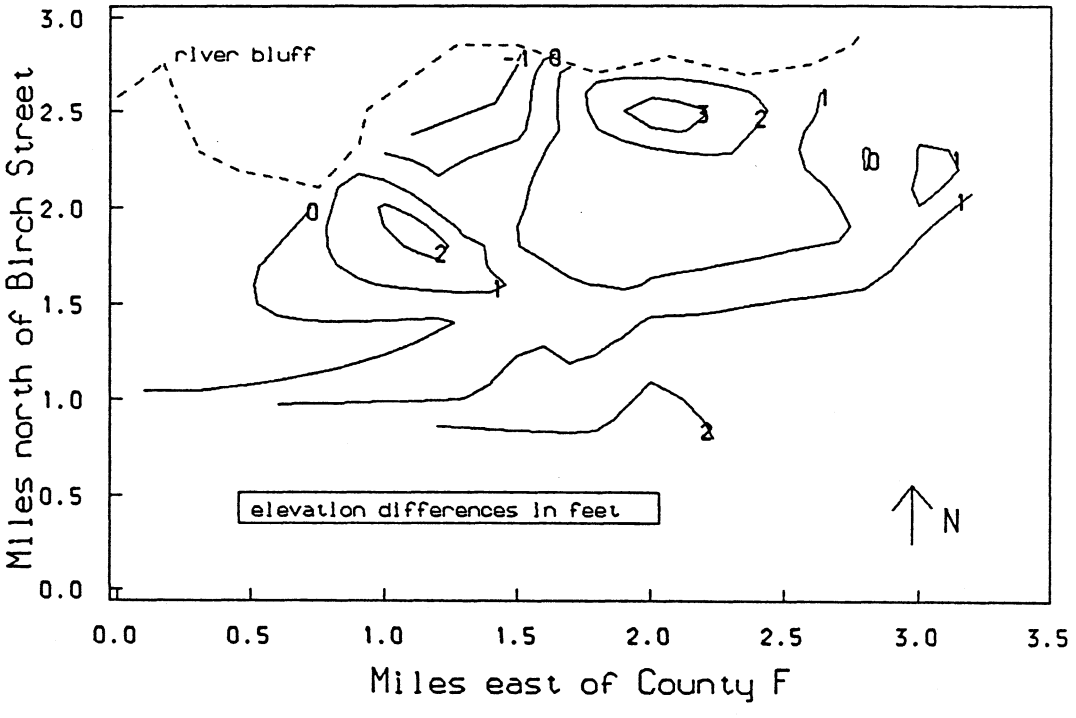

Figure 16. Map of differences in water table elevation from cubic fit to GPR data calibrated against well 440 and from linear interpolation of well data.

17 is a north-south cross section along Coolidge Avenue, which is 2.85 miles east of County Highway F. This cross section again shows the generally positive discrepancy between the radar-predicted and interpolated water tables. This discrepancy is also apparent in Figure 18, an east-west cross section along Prairie Drive, one mile north of Birch Street.

Figures 19 through 22 show the same series of comparisons between the interpolated water table and the radar-predicted water table as Figures 15 through 18 but based on the calibration against wells 440, 722 and 51. This radar-predicted water table (Figure 19) is slightly higher toward the north and about two feet lower toward the south than the one based on the calibration against well 440 alone (Figure 15). The difference shows up most clearly in the cross sections along Coolidge Avenue and Prairie Drive, which indicate that the radar-predicted water table is up to about a foot lower than the interpolated water table. However, from Figure 20 it is apparent that the radar-predicted water table based on this calibration is still generally higher than the interpolated water table, by as much as four feet.

Despite this positive bias in radar-predicted water table elevations, the radar-predicted water tables do show the same trends as the interpolated water table. The discrepancies are less than two feet in most areas. However, both radar-predicted maps fail to exhibit the expected groundwater divide. Evidence for the presence of the divide is apparent in the

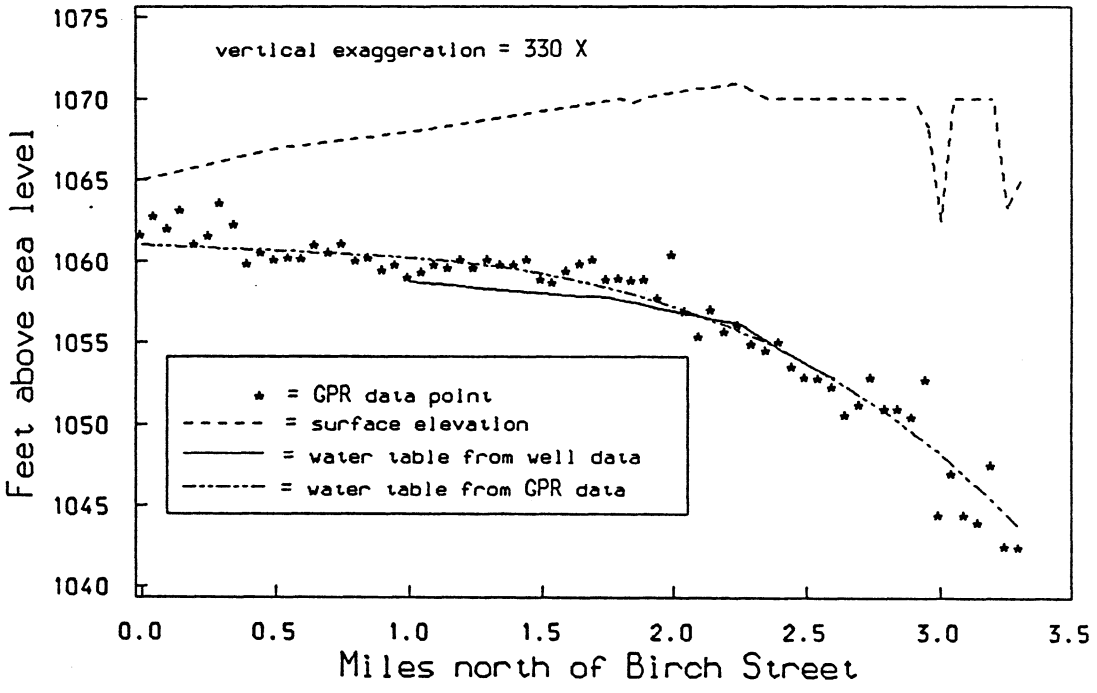

Figure 17. Cross section along Coolidge Avenue; GPR data are from calibration to well 440.

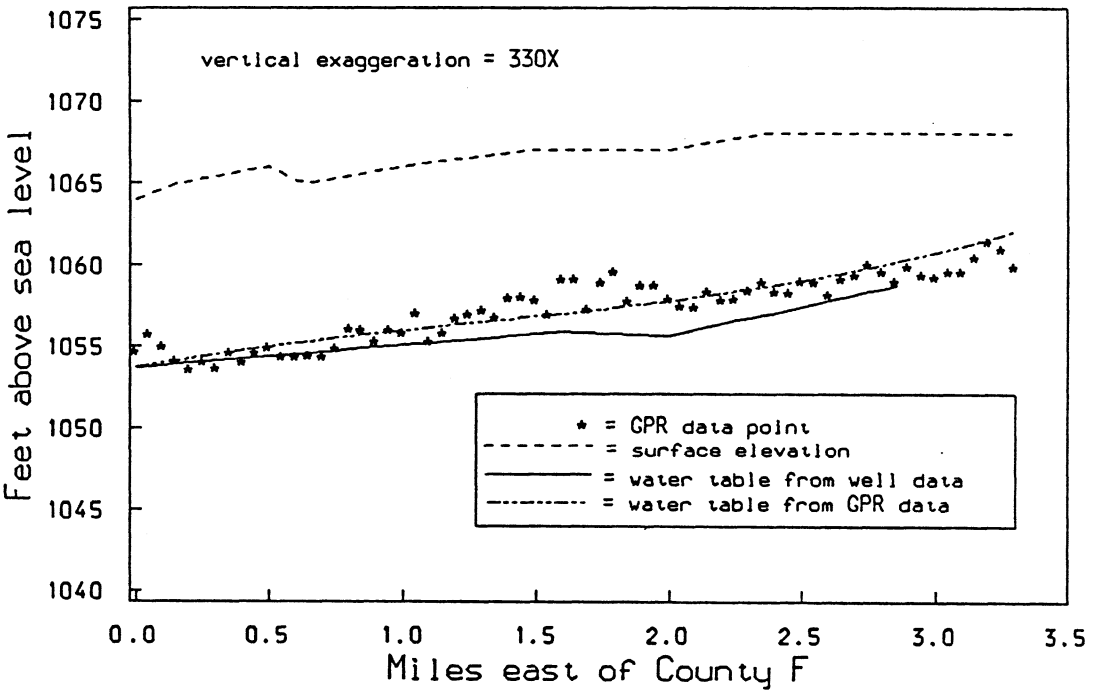

Figure 18. Cross section along Prairie Drive; GPR data are from calibration to well 440.

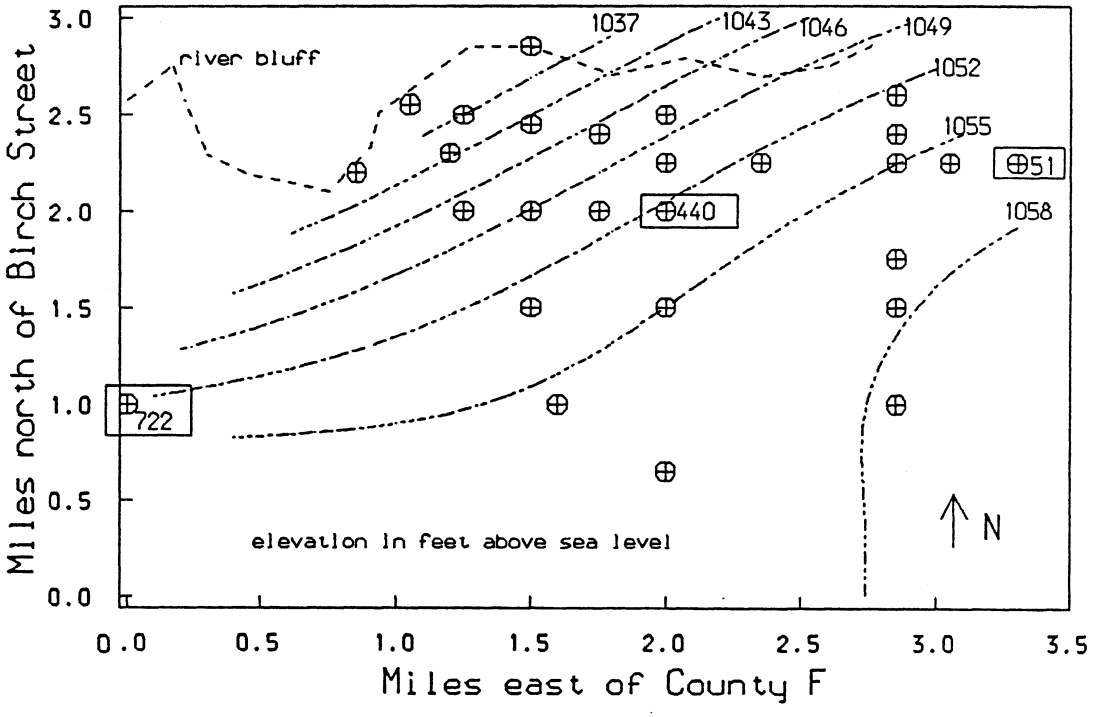

Figure 19. Water table map from cubic fit to GPR data calibrated against wells 440, 722 and 51.

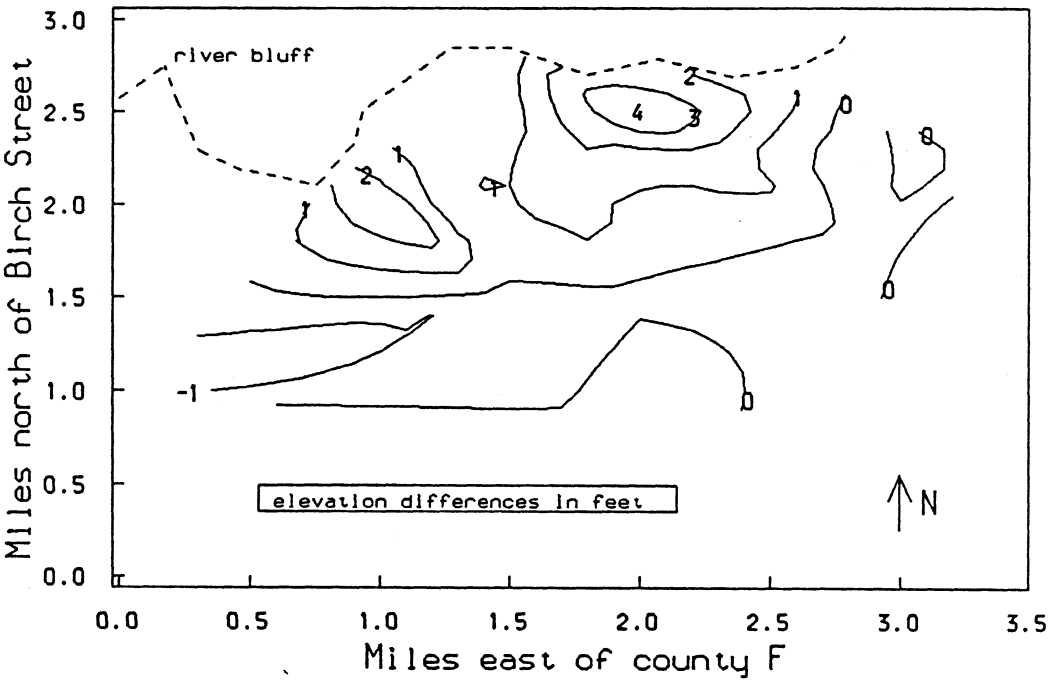

Figure 20. Map of differences in water table elevation from cubic fit to GPR data calibrated against wells 440, 722, and 51 and from linear interpolation of well data.

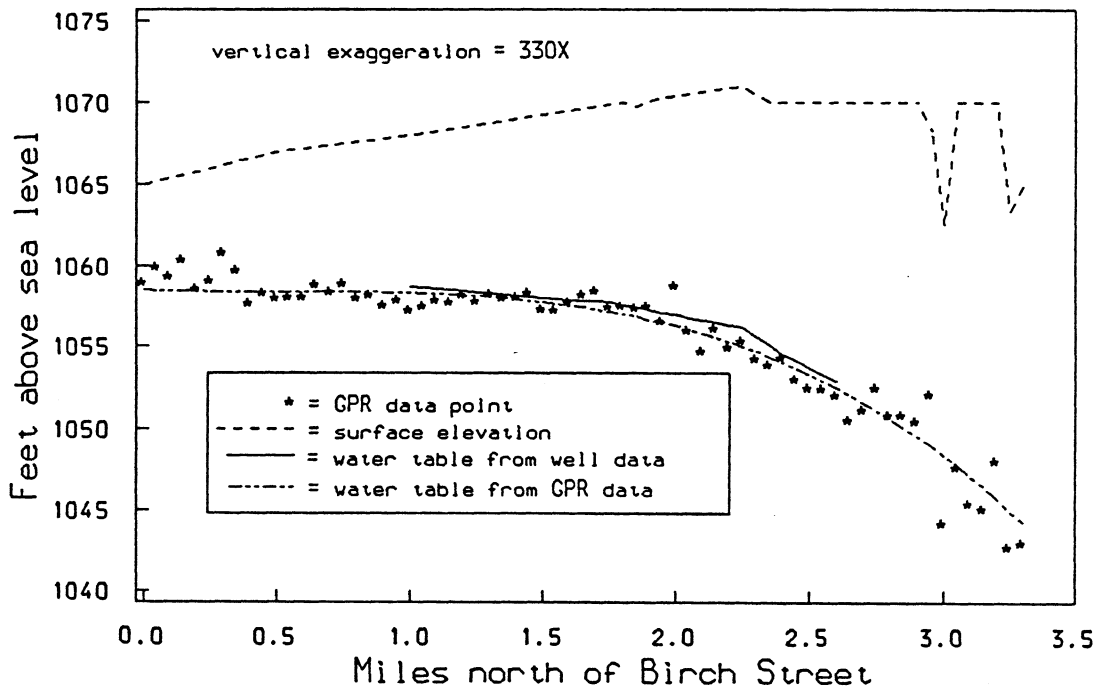

Figure 21. Cross section along Coolidge Avenue; GPR data are from calibration to wells 440, 722 and 51.

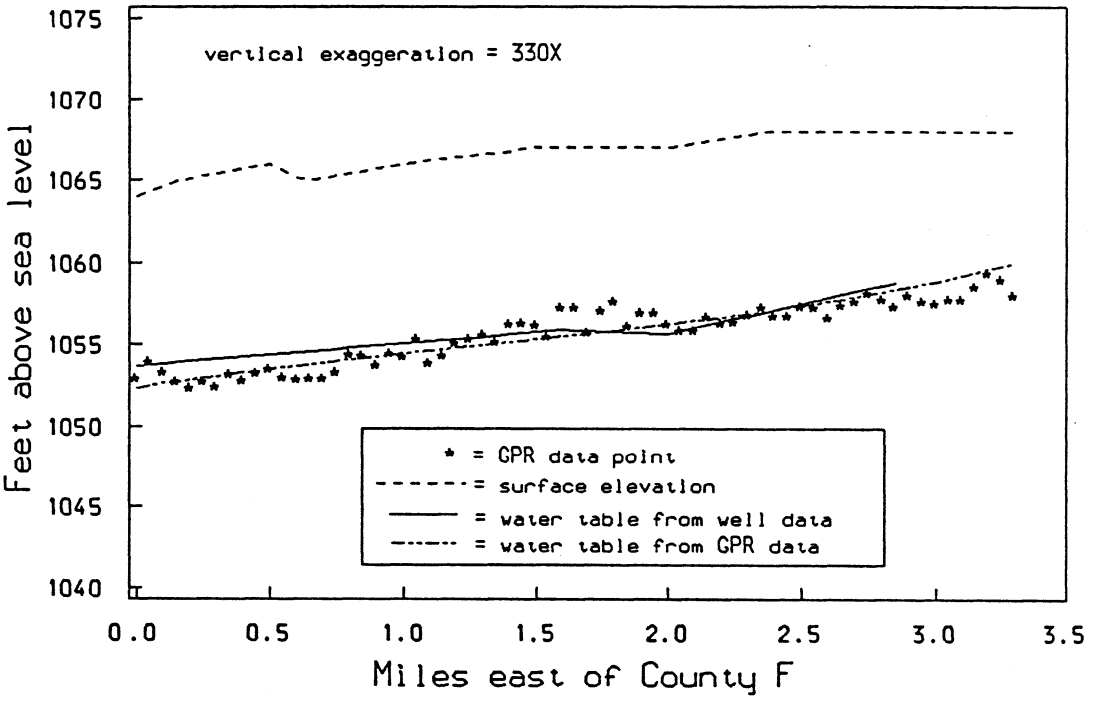

Figure 22. Cross section along Prairie Drive; GPR data are from calibration to wells 440, 722 and 51.

lines of radar data taken along Monroe Avenue, running north-south two miles east of County Highway F. However, there is no evidence for the presence of the divide in the data obtained along Coolidge Avenue and only weak evidence in the data obtained along Buchanan Avenue, 3.3 miles east of County Highway F. In the cross sections along Coolidge Avenue, one would expect the divide to be located between about 1.0 and 1.5 miles north of Birch Street. If the divide is present, the water table slope to the south of it does not make a large enough difference in the data to show up in the fitted surface.

In fact, Figures 17 and 21 show anomalously high values of radar-predicted water table elevation, relative to the fitted surface, at the southern end of Coolidge Avenue. These values are all within one-half mile of Ditch Number 1. It is possible that Ditch Number 1 was a losing rather than a gaining stream at this point at the time the radar surveys were made. In this case the water table would slope away from the ditch as shown and one would not expect to see a divide between the ditch and the river along this cross section. Faustini (1985) found that most drainage ditches in the Central Sand Plain are gaining streams throughout most of the year. Some, however, can become losing streams along certain reaches, especially in late fall and winter, as water levels decline throughout the sand plain.

Table 3 shows the correlation, root mean squared deviation, bias

Table 3. Correlation (cor), root mean squared deviation (rmsd), bias and maximum deviation (maxd) between GPR-generated water tables and water table from linear interpolation between observation wells for various sets of calibrating wells.

well set	cor	rmsd (ft)	bias (ft)	maxd (ft)
115	0.990	1.02	0.57	3.03
440	0.989	1.31	1.04	3.68
125	0.990	0.92	0.15	-2.80
108	0.990	0.97	0.43	2.84
440, 722	0.988	1.13	0.73	4.06
115,125	0.990	1.02	0.20	-3.17
440, 722, 51	0.986	1.08	0.40	4.01
115, 125, 122	0.990	0.99	0.48	2.87
440, 722, 51, 115, 125	0.989	0.92	0.48	3.20
440, 722, 51, 115, 125, 112, 104	0.989	0.87	0.41	3.32
all wells in Plainfield soils	0.989	0.82	0.28	3.04
all wells in Friendship soils	0.983	1.58	0.90	5.00
all 21 wells	0.989	0.81	0.25	3.10

and maximum deviation between radar-produced water tables and the interpolated water table for the same calibrating well sets as shown in Table 2. All the radar-predicted water tables show a positive bias with respect to the interpolated water table, consistent with the negative bias in radar-predicted depths. The results do not show a significant reduction in root mean squared deviation or bias with increasing calibrating set size. However, one would expect to reduce the chance of poorer results, such as those for well 440 (which yield a higher root mean squared deviation and bias), with increasing number of calibrating wells. This is because a larger set of calibrating wells is more likely to give calibration results that are representative of the entire area, as discussed in section D of this chapter.

VI. CONCLUSIONS AND SUGGESTIONS FOR FUTURE RESEARCH

A. Conclusions

The results in Table 2 indicate that accurate predictions of water table depth can be obtained from GPR data calibrated against a small number of wells. At least three wells are needed to obtain an estimate of the uncertainty in the two calibration parameters, radar signal velocity and return time correction factor. The most important source of variation in the calibration data about the fitted calibrating model is lateral variation in the radar signal velocity. Therefore, calibrating wells would ideally be located in areas where the most extreme contrasts in radar signal velocity are expected, based on existing knowledge of the distribution of soil types and subsurface materials. Such a distribution of calibrating wells would give a worst-case estimate of the variation in calibration parameters.

Most of the calibrating sets shown in Table 2 yielded a root mean squared deviation of about one foot and a correlation of about 0.99 between radar-predicted and observed depths at the remaining wells. These results do not show a strong dependence on the size of the calibrating set, although the root mean squared deviation between radar-predicted and observed depths resulting from calibrations against the sets of five and seven calibrating wells are notably lower than that for smaller sets.

The " optimal" number of calibrating wells will of course depend on the size of the study area and the expected degree of variation in the electromagnetic properties of the subsurface material. In the current study area, which is about nine square miles in area and characterized by quite uniform subsurface materials, three strategically placed calibrating wells are probably adequate to obtain a reasonable estimate of the uncertainty in the calibration parameters and to produce depth prediction results that are nearly as reliable as those from a calibration against a larger set of wells.

Radar-predicted depths can be subtracted from surface elevation values, smoothed and interpolated to produce maps of water table elevation. In this study, a cubic polynomial has been fit to radar-predicted water table elevations to produce radar-predicted water table maps for the study area. Table 3 contains the results of comparisons between radar-predicted water table maps resulting from calibrations against various well sets and the water table map produced by linear interpolation among the observation wells. For most calibrations, the root-mean squared deviation between the radar-predicted water table map and that produced from well data was about one foot, while the correlation between these two maps was about 0.99. However, the radar-predicted maps failed to reveal the presence of a groundwater divide which is thought to exist in the field area.

The radar signal quality appeared to be strongly influenced by minor changes in soil type in the field area. This result implies that GPR could be helpful in soil mapping studies, particularly in confirming and precisely delineating the boundaries between different soil types. However, this sensitivity of radar signal quality to minor changes in soil characteristics also implies that it is difficult to formulate guidelines for determining in advance where GPR surveys will prove successful and where they will be unsuccessful. If a certain area is known to have clay-rich soils, then an investigator can be fairly certain that GPR will yield no useful information in that area. Otherwise, trial-and-error may be the only means for determining whether the subsurface materials in an area can be successfully surveyed with radar methods. Fortunately, typical radar equipment is easily portable and reconnaissance radar surveys can be performed quickly. Thus, it is worthwhile to attempt radar surveys at sites of interest if radar equipment is available.

The results of the mass balance model employed in this study to calculate the distribution of groundwater recharge and discharge seemed to be strongly dependent on the interpolation technique employed to produce water table maps. No successful model runs based on observation well data were obtained and the results of model runs based on radar-predicted maps are unrealistic. As discussed in Appendix 1, two possible reasons for the failure of the mass balance technique in this study are: 1) the nodal

spacing chosen for the model (0.1 mile) was too small, making the model results overly sensitive to errors in the characterization of the water table slope; and 2) mass balance techniques, which were developed for modeling recharge/discharge patterns in regional groundwater basins, may not be appropriate for modeling an area as small as the current study area.

B. Suggestions for future research

A detailed study of the influence of water table interpolation techniques on the results of the mass balance model used in this study would not only help to clarify the reasons for the difficulties described in Appendix 1, but would also contribute to an understanding of mass balance modeling studies in general. In addition, using the data obtained in this study as input to an inverse model that does not require interpolation of data would help to isolate the influence of interpolation techniques on the mass balance model. One such model is described by Cooley (1977, 1982). The use of such a model would also provide a more objective comparison of recharge results based on observation well data and recharge results based on GPR data.

A systematic study of radar performance in various soil types would serve two purposes: 1) Such a study would evaluate the GPR's potential as a tool for mapping soil type boundaries. 2) In conjunction with county soil maps, the study results would provide a useful resource for planning

future GPR studies, indicating where radar surveys would be more or less likely to succeed.

REFERENCES CITED

Akima, Hiroshi. 1978. A method of bivariate interpolation and smooth surface fitting for irregularly distributed data points. ACM Transactions on Mathematical Software 4(2), pp. 148-159.

Annan, A. P., and J. L. Davis. 1976. Impulse radar sounding in permafrost. Radio Science 2(4), pp. 383-394.

Arcone, S. A. 1984. Field observations of electromagnetic pulse propagation in dielectric slabs. Geophysics 49(10), pp. 1763-1773.

Becker, R. A., and J. M. Chambers. 1984. S: An Interactive Environment for Data Analysis and Graphics. Wadsworth Advanced Book Program, Belmont, California, 550 pp.

Bogorodsky, V. V., C. R. Bentley and P. E. Gudmandsen. 1985. Radioglaciology. D. Reidel Publishing Company, Dordrecht, Holland, 254 pp.

Brownell, J. R. 1986. Stratigraphy of unlithified deposits in the Central Sand Plain of Wisconsin. University of Wisconsin, M.S. Thesis, 172 pp.

Clayton, L. 1986. Pleistocene geology of Portage County, Wisconsin. Wisconsin Geological and Natural History Survey Information Circular 56, 19 pp.

Cooley, R. L. 1977. A method of estimating parameters and assessing reliability for models of steady state groundwater flow, 1, Theory and numerical properties. Water Resources Research, 13(2), pp. 318-324.

Cooley, R. L. 1982. Incorporation of prior information on parameters into nonlinear regression groundwater flow models, 1, Theory. Water Resources Research 18(4), pp. 965-976.

Davis, J. L., and W. J. Chudobiak. 1975. In situ meter for measuring relative permittivity of soils. Geological Survey of Canada, Paper 75-1, Part A, pp. 75-79.

Davis, J. L., R. W. D. Killey, A. P. Annan and C. Vaughan. 1984. Surface and borehole ground-penetrating radar surveys for mapping

geological structures. Proceedings of the National Water Well Association/Environmental Protection Agency Conference on Surface and Borehole Geophysical Methods in Ground Water Investigations, February 7-9, 1984, San Antonio, Texas, pp. 681-712.

Draper, N. R., and H. Smith. 1981. Applied Regression Analysis, Second Edition. John Wiley & Sons, New York, 709 pp.

Faustini, J. M. 1985. Delineation of groundwater flow patterns in a portion of the Central Sand Plain of Wisconsin. University of Wisconsin, M.S. Thesis, 117 pp.

Freeze, R. A. 1967. Quantitative interpretation of regional groundwater flow patterns as an aid to water balance studies. International Association of Scientific Hydrology, General Assembly of Berne, Publication 77, pp. 154-173.

Freeze, R. A., and P. A. Witherspoon. 1968. Theoretical analysis of regional groundwater flow - 3. Quantitative interpretations. Water Resources Research 4(3), pp. 581-590.

Freeze, R. A. and J. A. Cherry. 1979. Groundwater. Prentice-Hall, Inc., Englewood Cliffs, N.J., 604 pp.

Haeni, F. P., D. K. Mckeegan and D. R. Capron. 1987. Ground-penetrating radar study of the thickness and extent of sediments beneath Silver Lake, Berlin and Meriden, Connecticut. U. S. Geological Survey Water-Resources Investigations Report 85-4108, 19 pp.

Harkin, J. M., G. Chesters, F. A. Jones, R. N. Fathulla, E. K. Dzantor and D. G. Kroll. 1986. Fate of aldicarb in Wisconsin groundwater. University of Wisconsin, Water Resources Center, Technical Report WIS WRC 86-01, 49 pp.

Holt, C. L. R., Jr. 1965. Geology and water resources of Portage County, Wisconsin. U. S. Geological Survey Water-Supply Paper 1796, 77 pp.

Horton, K. A., R. M. Morey, R. H. Beers, V. Jordan, S. S. Sandler and L. Isaacson. 1981. An evaluation of ground penetrating radar for assessment of low level nuclear waste disposal sites. Office of Nuclear Regulatory Research, Nuclear Regulatory Commission,

Report number NUREG/CR-2212.

Houck, R. T. 1984. Measuring moisture content profiles using ground-probing radar. Proceedings of the National Water Well Association/Environmental Protection Agency Conference on Surface and Borehole Geophysical Methods in Ground Water Investigations, February 7-9, 1984, San Antonio, Texas, pp. 637-653.

Karnauskas, R. J. 1977. The hydrogeology of the Nepco Lake watershed in central Wisconsin with a discussion of management implications. University of Wisconsin, M.S. Thesis, 249 pp.

King, R. W. P., and G. S. Smith. 1981. Antennas in Matter: Fundamentals, Theory, and Applications. The MIT Press, Cambridge, Massachusetts, 868 pp.

Kraft, G. J., In preparation. Contaminant hydrogeology of aldicarb residues in a groundwater basin near Plover, Wisconsin. University of Wisconsin, Ph.D. Thesis.

McDonald, M. G. and A. W. Harbaugh. 1984. A modular three-dimensional finite-difference ground-water flow model. U. S. Geological Survey Open-File Report 83-875, 528 pp.

Muldoon, M. A. 1987. Hydrogeologic and geotechnical properties of prelate Wisconsin till units in western Marathon County, Wisconsin. University of Wisconsin, M.S. Thesis, 251 pp.

Murray, W. A. and P. L. Monkmeyer. 1973. Validity of Dupuit-Forchheimer equation. Journal of the Hydraulics Division, Proceedings of the American Society of Civil Engineers, 99(HY9), pp. 1573-1583.

Neuman, S. P., and S. Yakowitz. 1979. A statistical approach to the inverse problem of aquifer hydrology, 1, Theory. Water Resources Research, 15(4), pp. 845-860.

Neuman, S. P. 1980. A statistical approach to the inverse problem of aquifer hydrology, 3, Improved solution method and added perspective. Water Resources Research, 16(2), pp. 331-346.

Olhoeft, G. R. 1986. Direct detection of hydrocarbons and organic chemicals with ground penetrating radar and complex resistivity.

Proceedings of the National Water Well Association Conference on Petroleum Hydrocarbons and Organic Chemicals in Ground Water, Nov. 12-14, 1986, Houston, pp. 284-305.

Otter, A. J., and W. D. Fiala. 1978. Soil Survey of Portage County, Wisconsin. United States Department of Agriculture, Soil Conservation Service, 96 pp.

Rothschild, E. R., R. J. Manser and M. P. Anderson. 1982. Investigation of aldicarb in ground water in selected areas of the Central Sand Plain of Wisconsin. Ground Water 20(4), pp. 437-445.

Sakayama, T., T. Hara and T. Imai. 1983. Study of the combined use of ground penetrating radar and electric profiling in soil exploration. Bulletin of the International Association of Engineering Geology 26, pp. 309-313.

Shih, S. F., J. A. Doolittle, D. L. Myhre and G. W. Schellentrager. 1986. Using radar for groundwater investigation. Journal of Irrigation and Drainage Engineering 112(2), pp. 110-118.

Stoertz, M. W. 1985. Evaluation of groundwater recharge in the Central Sand Plain of Wisconsin. University of Wisconsin, M.S. Thesis, 159 pp.

Stoertz, M. W. and K. R. Bradbury. 1988. Mapping recharge areas using a groundwater flow model - a case study, Ground Water, in review.

Topp, G. C., J. L. Davis and A. P. Annan. 1980. Electromagnetic determination of soil water content: measurements in coaxial transmission lines. Water Resources Research 16(3), pp. 574-582.

Ulriksen, C. P. F. 1982. Application of impulse radar to civil engineering. Lund University of Technology, Lund, Sweden, Ph.D. Thesis, 175 pp.

Underwood, J. E. and J. W. Eales. 1984. Detecting a buried crystalline waste mass with ground-probing radar. Proceedings of the National Water Well Association/Environmental Protection Agency Conference on Surface and Borehole Geophysical in Ground Water Investigations, February 7-9, 1984, San Antonio, Texas, pp. 654-665.

Wartenberg, D. 1988. Groundwater contamination by Temik aldicarb

pesticide: The first 8 months. Water Resources Research 24(2), pp. 185-194.

Weeks, E. P. 1969. Determining the ratio of horizontal to vertical permeability by aquifer test analysis. Water Resources Research 5(1), pp. 196-214.

Weeks, E. P., and M. L. Sorey. 1973. Use of finite-difference arrays of observation wells to estimate evapotranspiration from ground water in the Arkansas River Valley, Colorado. U. S. Geological Survey Water-Supply Paper 2029-C, 27 pp.

Weeks, E. P. and H. G. Stangland. 1971. Effects of irrigation on streamflow in the Central Sand Plain of Wisconsin. U. S. Geological Survey Open-File Report, 113 pp.

Wright, D. L., G. R. Olhoeft and R. D. Watts. 1984. Ground-penetrating radar studies on Cape Cod. Proceedings of the National Water Well Association/Environmental Protection Agency Conference on Surface and Borehole Geophysical Methods in Ground Water Investigations, February 7-9, 1984, San Antonio, Texas, pp. 666-680.

Yeh, W. W-G. 1986. Review of parameter identification procedures in groundwater hydrology: The inverse problem. Water Resources Research, 22(2), pp. 95-108.

APPENDIX 1: RECHARGE MODELING RESULTS

A. Introduction

The radar-generated water table maps discussed in Chapter V were used as input to a mass balance model which calculates the distribution of recharge and discharge based on a specified water table configuration. This appendix briefly discusses the details of the model employed in this study and presents the results of the modeling. The results in this case appear to be highly dependent on the interpolation technique used to calculate water table elevation at all the nodes in the model. Thus, the particular results presented here should be regarded with some degree of skepticism.

B. Recharge Modeling Technique

Groundwater flow is governed by a partial differential equation in which the dependent variable is groundwater head (potential energy per unit weight of water). For an unconfined aquifer, the parameters in this equation include the hydraulic conductivity and specific yield of the aquifer (both of which may vary spatially) and sink/source terms such as pumping rates and recharge rates (which may vary with both space and time). Solving the forward problem involves specifying the distribution of the necessary parameters, boundary conditions and initial conditions (for transient problems) and solving either analytically or numerically for the

distribution of head. One can attempt to determine parameter values in a certain area by successively solving such a model, systematically varying the values of one or more parameters, until calculated heads match observed heads to some degree of accuracy. However, this method of parameter estimation is time-consuming. It is also non-unique if more than one parameter is considered unknown.

The inverse method of parameter estimation involves specifying head values within the problem domain and solving for parameter values directly. Inverse models are described by Neuman and Yakowitz (1979), Neuman (1980), Cooley (1977, 1982) and Yeh (1986). One could consider a mass balance accounting scheme as a kind of inverse model. In particular, if the hydraulic conductivity of an unconfined aquifer is considered known and steady state conditions apply, the distribution of recharge and discharge can be determined from a map (or profile, for a cross-sectional problem) of water table elevation (e.g., Weeks and Sorey, 1973; Freeze, 1967; Freeze and Witherspoon, 1968). Under steady state conditions, water table elevation is approximately equal to head given that the slope of the water table is no greater than 1:10 (Murray and Monkmeyer, 1973). Stoertz and Bradbury (1988) modified the USGS Modular Groundwater Flow Model (McDonald and Harbaugh, 1984) to determine the distribution of recharge based on mass-balance calculations given that water table elevation, hydraulic conductivity and aquifer thickness are specified

throughout the problem domain. This program is used for the recharge calculations done in this study. The details of the modifications to the code and an application of the model to the Buena Vista Groundwater Basin are presented in Stoertz and Bradbury (in review).

It should be noted that the inverse approach is also non-unique if more than one parameter is considered unknown. Calibration of the model against field observations, such as measured discharge to streams, or incorporation of prior information on aquifer parameters (Cooley, 1982) can help to constrain the solution of an inverse model. In this study hydraulic conductivity is treated as a known quantity, so that recharge is the only unknown parameter.

C. Details of the Mass Balance Model

In the present study, the mass balance model is applied in areal view in two dimensions. Every node in the model is assigned a value of water table elevation, aquifer bottom elevation and hydraulic conductivity. The model then uses Darcy's law to calculate the flux across each of the four sides of each nodal cell, based on the hydraulic gradients between that cell and the adjacent cells, the value of hydraulic conductivity and the saturated thickness of the aquifer. A mass balance surplus at a given cell is interpreted as recharge, that is, as downward flux of water across the water table from above. A mass balance deficit is interpreted as

discharge across the water table.

In this study, all nodes in the model were assigned a hydraulic conductivity value of 320 $\frac{ft}{day}$, the value obtained from a pump test (Weeks, 1969; Weeks and Stangland, 1971) in the central part of the study area (Figure 2). The recharge and discharge rates calculated are directly proportional to the value of hydraulic conductivity specified. If the aquifer is assumed to be homogeneous, however, the calculated recharge/discharge pattern is not dependent on the value of the hydraulic conductivity (Stoertz and Bradbury, in review). Stoertz and Bradbury report that the geometric mean of hydraulic conductivity values from pump tests in and near the Buena Vista Groundwater Basin is 260 $\frac{ft}{day}$ and use this value in their mass balance model. As mentioned in Chapter II, the sediments in the present study area tend to be coarser than average for the Central Sand Plain, so one would expect a higher hydraulic conductivity here.

The elevation of the bottom of the aquifer is taken to be 1000 feet above sea level for every node in the model. Although this is a simplification of reality (see Chapter 2), the resulting pattern of saturated thickness is similar to that mapped by Kraft (in preparation) from field data.

D. Model Dependence on Interpolation Techniques

The original intent of this study was to compare recharge/discharge distributions calculated from radar-predicted water tables to the recharge/discharge distribution calculated from the water table interpolated from well data. Several interpolation techniques were used to produce nodal water table elevation values from the well data, including simple linear interpolation, a method based on triangulating the data points and fitting a fifth order polynomial within each triangle (Akima, 1978) and inverse distance squared-weighted interpolation. The results of the mass balance model in each case were chaotic, with very large recharge values and very large discharge values occurring at immediately adjacent nodes. One might expect such a result for calculations based on a water table map produced by linear interpolation, since such a water table exhibits a discontinuous slope and the model tends to produce a recharge/discharge pair at every break in slope. However, the other two methods produce fairly smooth surfaces. Akima's method, in fact, is designed to produce a surface that is not only continuous but has a continuous first derivative. It is possible that, because discrete values from this theoretically smooth surface are the actual input to the mass balance model, the model treats rapid changes in slope as breaks in slope. Because of these problems, no reasonable recharge results based on well data were obtained.

Two methods for interpolating the GPR-predicted elevations were tested. The first method involved smoothing the individual lines of data

and then using inverse distance-squared weighted interpolation to produce a water table surface based on the smoothed data. This also produced a chaotic recharge/discharge pattern. The method chosen for this study, fitting a cubic polynomial to the entire set of data, was chosen primarily because it produced reasonable recharge/discharge results. Since the polynomial is fit globally, it is smooth throughout the problem domain. As described in Chapter V, the fitted equation is used to calculate water table elevations at all the nodes in the model grid. The nodal spacing is one-tenth of a mile in both the east-west and north-south directions. Thus the entire study area, which is 3.3 miles on a side, is represented by a 34 by 34 array of nodes. However, nodes which are outside the polygon surrounding the radar survey points are ignored by the model.

In their application of the mass balance recharge modeling technique to the Buena Vista Groundwater Basin, Stoertz and Bradbury (in review) obtained results which agreed well with the recharge/discharge pattern mapped on the basis of field evidence (Faustini, 1985). In their study, nodal values of water table elevation were interpolated by hand from piezometer data distributed throughout the 170 square mile basin. They report that calculated recharge/discharge rates were quite sensitive to the nodal spacing employed in the model, although the recharge/discharge pattern was less sensitive to nodal spacing. The average recharge rate calculated using a " fine" nodal grid, with variable

nodal spacings ranging from 0.25 to 0.5 miles, was 24.1 $\frac{in}{yr}$, whereas the average recharge rate calculated using a " coarse" nodal grid, with nodal spacings ranging from 1 to 2 miles, was 8.0 $\frac{in}{yr}$. Stoertz and Bradbury attribute this decrease in the calculated magnitude of recharge (and discharge) with increasing coarseness of the model grid to a smoothing out of the irregularities in the water table. They state, " The calculated fluxes in the coarse model are smaller because local flow paths are shorter than the cell spacing. In effect, some water is recharged and then discharged again within a single cell." Thus, choosing the appropriate level of discretization is important to obtaining accurate results from a mass balance model.

The above findings suggest two possible reasons for the sensitivity of recharge results to interpolation technique in the current study. First, because the flux value calculated between two nodes is directly proportional to the difference in head between the two nodes, the accuracy of model results is strongly dependent upon the accuracy of characterization of the water table slope between nodes. As nodal spacing decreases, the head differences between nodes will decrease. Because the relative error in the difference between two values can become quite large as the value of the difference decreases, an accurate characterization of the water table slope becomes even more important as nodal spacing decreases.

Furthermore, the sensitivity of recharge results to differences in head increases with increasing hydraulic conductivity. Neuman and Yakowitz (1979) discuss these problems as they relate to inverse modeling to determine aquifer transmissivities. This could imply that, for a given hydraulic conductivity, there is a certain value of nodal spacing below which mass balance modeling results become overly sensitive to the interpolation technique used to generate nodal values of water table elevation. In particular, as nodal spacing decreases and hydraulic conductivity increases, the effects of breaks in the slope of the input water table would become more dramatic. Perhaps the nodal spacing employed in this study, 0.1 mile, was too small for the value of hydraulic conductivity employed, giving rise to the large number of recharge/discharge pairs occurring at immediately adjacent nodes.

Initial modeling attempts based on the radar data actually employed a nodal spacing of 0.05 miles. The nodal spacing was increased to 0.1 mile to decrease the model run time. This change in nodal spacing did, in fact, produce a smoother recharge/discharge pattern, even though the same cubic polynomial was used to produce the nodal values of water table elevation in both cases. This suggests that model results are fairly sensitive to nodal spacing in this case.

A second possible reason for the failure of the model to produce reasonable results, especially in the case of the well data, is that mass balance

modeling may not be appropriate for a study area of this size, approximately nine square miles. This reason is closely related to the first, since the nodal spacing will generally decrease as the scale of the problem decreases. Interpolating well data to produce a regional scale water table map will almost always involve some degree of spatial averaging, or smoothing out, of small-scale features, as mentioned by Stoertz and Bradbury. It is possible that a mass balance approach is most appropriately applied to just such a spatially averaged surface. Small-scale irregularities in the water table would often correspond to localized, transient events. Thus, the spatial averaging associated with creating a regional water table map also implicitly involves a kind of temporal averaging. This spatially/temporally averaged regional water table would be more likely to represent the steady state conditions required for the application of mass balance modeling than would a water table map for a smaller area. Alternatively, as the water table is represented in more detail, transient effects become more apparent and a steady state analysis becomes less appropriate. It is possible that the assumption that the interpolated water table maps represent steady state conditions (Chapter II) is not valid, at least at this scale of analysis.

E. Recharge Model Results

Figures 23 and 24 show the recharge/discharge pattern calculated

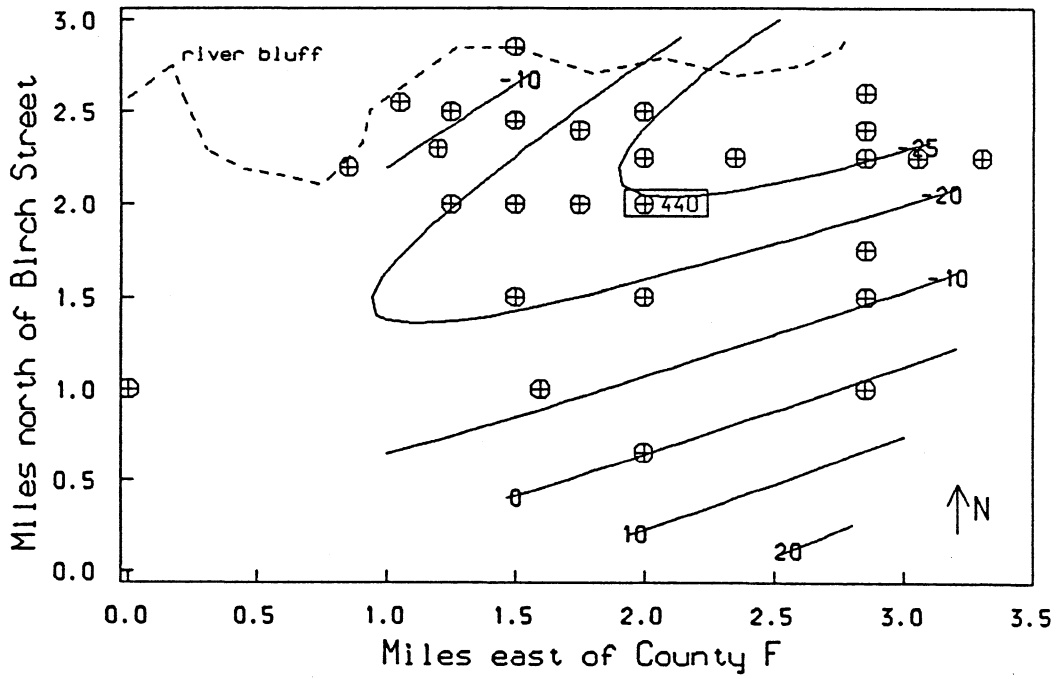

Figure 23. Recharge/discharge rates in in/yr calculated from water table fit to GPR data calibrated to well 440. Negative values are discharge and positive are recharge.

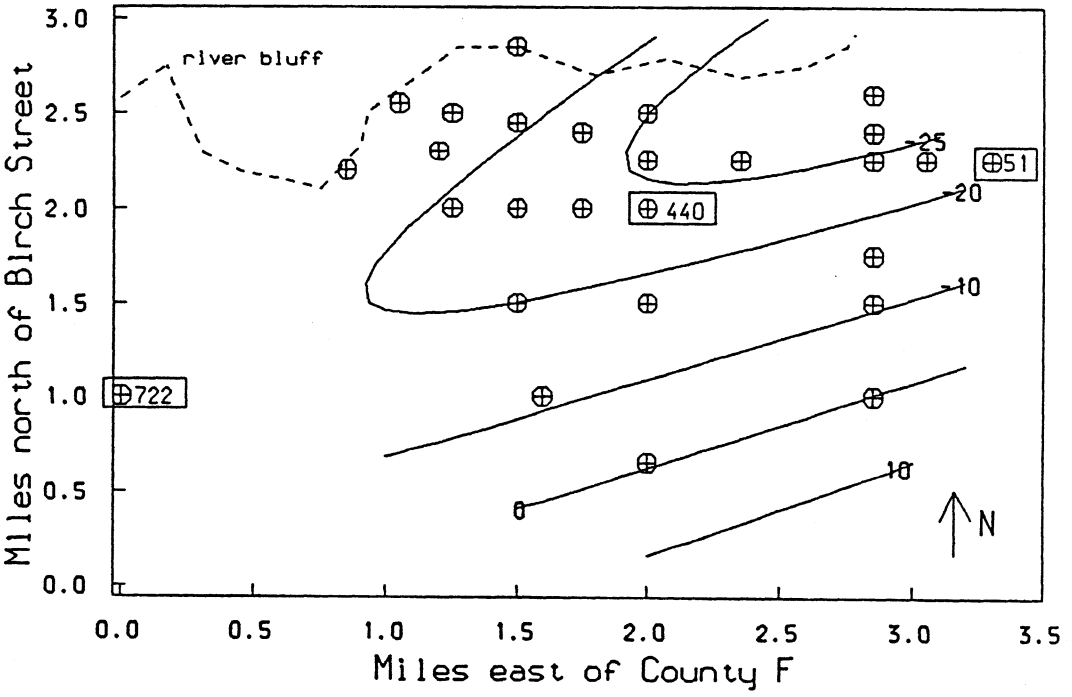

Figure 24. Recharge/discharge rates in in/yr calculated from water table fit to GPR data calibrated to wells 440, 722 and 51. Negative values are discharge and positive are recharge.

by the mass balance model based on the radar-predicted water tables produced by the calibrations against well 440 and against wells 440, 722 and 51, respectively. The results are almost identical. Since the radar-predicted water tables all have the same functional form, with only slight variations in the particular parameters in the fitted cubic equation, the model is bound to produce nearly identical recharge/discharge patterns for all the water tables.

The modeled recharge/discharge pattern also seems unrealistic. In a regional groundwater basin, such as the Buena Vista Groundwater Basin, recharge generally occurs over a broad area and discharge is generally concentrated near surface water bodies and wetlands. Average recharge rates are generally lower than average discharge rates. The increased area of recharge compensates for the lower recharge rates, yielding an overall mass balance for the basin. For the modeled pattern, total discharge exceeds total recharge, probably because the modeled region does not correspond to a regional basin. However, assuming that Drainage Ditch Number 1 is a gaining stream, one would expect to see a broad area of recharge in the central portion of the study area, with discharge concentrated near the bluff along the Wisconsin River to the north and along Drainage Ditch Number 1 to the south. The model results represent a reasonable approximation of reality only if no divide existed between Drainage Ditch Number 1 and the Wisconsin River at the time the radar data were collected

(November, 1987). In this case, water would be flowing into the study area from the south. In either case, one would expect discharge rates to increase continuously toward the bluff. The modeled discharge rates increase and then decrease again with toward the bluff.

Table 4 contains a numerical summary of the results of the mass balance model for the radar-predicted water tables produced from calibrations against the various well sets. As expected, there is little variation in the model results, especially in terms of the percentage of the modeled area occupied by recharge and discharge and the maximum and mean discharge rates calculated. The mean discharge rates vary between 16.33 and 17.47 $\frac{in}{yr}$. This agrees well with the average modeled discharge of 17.6 $\frac{in}{yr}$ for the Buena Vista Groundwater Basin reported by Stoertz and Bradbury (in review). However, the average recharge rates shown in Table 4 are notably lower than their calculated average recharge, 13 $\frac{in}{yr}$. Again, part of the reason for this discrepancy is that the current study area does not represent a regional basin. For the same reason, a net basin yield, given by the total discharge divided by total basin area, cannot be calculated for the modeled area.

Table 4. Summary of recharge modeling results for mass balance modeling based on GPR-generated water tables for various calibrating well sets; results shown are percent of modeled area occupied by recharge and discharge and maximum and mean recharge/discharge rates.

	Recharge (in/yr)			Discharge (in/yr)		
well set	% area	max	mean	% area	max	mean
115	16	23.02	8.79	84	29.08	16.97
440	16	22.59	8.65	84	29.45	17.27
125	16	23.40	8.99	84	28.73	16.66
108	16	23.14	8.85	84	28.97	16.87
440, 722	15	20.29	7.77	85	29.26	17.33
115, 125	16	24.01	9.20	84	28.73	16.58
440, 722, 51	15	19.27	7.36	85	29.04	17.24
115, 125, 122	16	23.19	8.88	84	29.00	16.88
440, 722, 51, 115, 125	16	22.10	8.43	84	29.05	17.05
440, 722, 51, 115, 125, 112, 104	16	21.51	8.13	84	29.00	17.11
all wells in Plainfield soils	16	21.94	8.35	84	28.90	16.97
all wells in Friendship soils	15	18.00	6.87	85	29.40	17.47
all 21 wells	16	21.62	8.20	84	28.89	17.01

APPENDIX 2: PIEZOMETER CODES

The piezometers labeled 100-181 in this study were installed during 1986 and 1987 for the ongoing study by Kraft (in preparation) and the labels used in this study for these piezometers are identical to those used by Kraft. The following piezometers, installed for earlier studies, were assigned numerical codes in this study which are different from their original labels, as shown. DNR is the Wisconsin Department of Natural Resources, WGNHS is the Wisconsin Geological and Natural History Survey and Harkin is Professor John M. Harkin and others of the University of Wisconsin-Madison. The information is from Kraft (in preparation).

installed by	date installed	original label	code for this study
DNR	1985	R-1	1
DNR	1985	R-2	2
DNR	1985	OW-1	3
DNR	1985	OW-2	4
WGNHS	1976	K-44	440
———	———	GS-722	722
Harkin	1981	1A	11
Harkin	1981	1B	12
Harkin	1981	1C	13
Harkin	1981	2A	21
Harkin	1981	2B	22
Harkin	1981	3A	31
Harkin	1981	3B	32
Harkin	1981	5A	51
Harkin	1981	5B	52
Harkin	1981	6A	61
Harkin	1981	6B	62
Harkin	1981	9A	91
Harkin	1981	9B	92
Harkin	1981	11A	5

APPENDIX 3: PIEZOMETER CONSTRUCTION DATA

The values for measuring point (m.p.) elevation, bottom elevation and screen length are from Kraft (in preparation). For those piezometers next to roads where GPR surveys were performed, the last column (del) gives the difference in elevation between the measuring point of the piezometer and the road surface next to the piezometer.

piez. code	mi. E of County F	mi. N of Birch St.	m.p. el. (ft asl)	bottom el. (ft asl)	screen length (ft)	del (ft)
722	0.00	1.00	1065.3	———	———	1.318
100	0.85	2.20	1064.9	993.6	5.0	———
102	0.85	2.20	1064.6	1017.5	5.0	———
101	0.85	2.20	1064.8	1033.4	5.0	———
116	1.05	2.55	1062.3	1033.2	5.0	———
119	1.20	2.30	1066.6	1037.9	5.0	———
117	1.20	2.70	1064.7	1030.5	5.0	———
177	1.25	2.00	1068.0	1018.6	5.0	1.355
178	1.25	2.00	1067.4	1028.8	5.0	0.795
122	1.25	2.00	1068.4	1041.7	5.0	1.575
118	1.25	2.50	1064.8	1035.4	5.0	———
140	1.50	1.50	1070.1	1006.2	5.0	1.882
142	1.50	1.50	1070.4	1030.0	5.0	2.117
172	1.50	1.50	1070.4	1031.6	5.0	1.944
141	1.50	1.50	1070.3	1036.0	5.0	———
126	1.50	1.50	1070.1	1049.5	5.0	1.812
139	1.50	2.00	1070.1	1005.3	5.0	2.097
137	1.50	2.00	1069.8	1022.7	5.0	1.789
138	1.50	2.00	1070.2	1037.4	5.0	2.124
123	1.50	2.00	1069.2	1043.3	5.0	1.121
120	1.50	2.40	1068.7	1034.1	5.0	0.713
103	1.50	2.85	1068.0	1013.8	5.0	2.057
104	1.50	2.85	1066.9	1032.3	5.0	0.895
109	1.60	1.00	1067.8	992.5	5.0	1.477
110	1.60	1.00	1067.6	1024.1	5.0	1.182
176	1.60	1.00	1067.5	1029.4	5.0	1.242
111	1.60	1.00	1067.5	1054.2	5.0	1.214
134	1.75	2.00	1070.4	1014.8	5.0	1.092
136	1.75	2.00	1070.0	1025.5	5.0	0.664
135	1.75	2.00	1070.1	1036.0	5.0	0.779
124	1.75	2.00	1070.1	1044.9	5.0	0.756
106	1.75	2.40	1069.0	1032.1	5.0	———
113	2.00	0.65	1067.8	1002.8	5.0	2.248
112	2.00	0.65	1067.7	1054.2	5.0	2.222

piez. code	mi. E of County F	mi. N of Birch St.	m.p. el. (ft asl)	bottom el. (ft asl)	screen length (ft)	del(ft)
107	2.00	1.50	1070.8	1010.9	5.0	1.449
143	2.00	1.50	1070.0	1028.8	5.0	0.689
175	2.00	1.50	1070.5	1039.8	5.0	1.149
108	2.00	1.50	1069.8	1053.1	5.0	0.466
440	2.00	2.00	1072.3	1040.5	1.5	2.688
2	2.00	2.25	1072.9	1024.7	3.0	1.770
1	2.00	2.25	1073.2	1034.2	3.0	2.045
105	2.00	2.50	1070.7	1007.0	5.0	———
4	2.00	2.50	1071.3	1022.1	5.0	———
3	2.00	2.50	1070.8	1032.6	5.0	———
121	2.00	2.70	1068.9	1040.5	5.0	———
130	2.35	1.70	1070.3	1025.6	5.0	———
129	2.35	1.70	1070.0	1040.0	5.0	———
131	2.35	1.70	1069.5	1040.7	5.0	———
127	2.35	1.70	1069.6	1051.6	5.0	———
179	2.35	2.25	1070.8	1026.7	5.0	1.594
133	2.35	2.25	1070.2	1035.8	5.0	0.966
125	2.35	2.25	1070.8	1046.9	5.0	1.538
132	2.35	2.25	1070.2	1051.6	5.0	1.024
114	2.85	1.00	1069.1	999.3	5.0	1.207
115	2.85	1.00	1069.1	1056.3	5.0	1.191
180	2.85	1.50	1069.7	1029.5	5.0	0.440
181	2.85	1.50	1069.7	1041.1	5.0	0.480
128	2.85	1.50	1069.8	1054.2	5.0	0.581
62	2.85	1.75	1071.2	1050.1	1.0	1.660
61	2.85	1.75	1072.8	1051.7	1.0	3.360
32	2.85	2.25	1074.1	1037.0	1.0	2.880
31	2.85	2.25	1074.4	1053.3	1.0	3.252
5	2.85	2.40	1072.1	1053.0	1.0	1.334
13	2.85	2.60	1072.2	1023.2	1.0	1.901
12	2.85	2.60	1072.7	1046.6	1.0	2.381
11	2.85	2.60	1073.2	1055.5	1.0	2.904
91	3.05	2.25	1069.7	1052.5	1.0	0.282
92	3.05	2.25	1071.2	1053.8	1.0	1.834
22	3.05	2.60	1073.5	1036.2	1.0	———
21	3.05	2.60	1074.5	1053.3	1.0	———
52	3.30	2.25	1072.9	1038.7	1.0	2.028
51	3.30	2.25	1074.0	1053.9	1.0	3.088
72	3.30	2.60	1072.1	1035.9	1.0	———
71	3.30	2.60	1072.9	1052.8	1.0	———

APPENDIX 4: DEPTH TO WATER IN PIEZOMETERS

Measurements for 10/87 are from Kraft (in preparation).

Depths to water in feet

	date				
piez. code	10/2/87	10/23/87	10/24/87	11/3/87	11/6/87
1	NA	NA	24.170	NA	24.270
2	NA	NA	24.440	NA	24.515
3	27.020	27.030	NA	27.020	NA
4	NA	27.500	NA	27.540	NA
5	NA	NA	NA	17.565	NA
11	NA	NA	NA	NA	NA
12	NA	NA	NA	19.850	NA
13	NA	NA	NA	19.475	NA
31	NA	NA	NA	18.282	NA
32	NA	NA	NA	17.905	NA
51	NA	NA	NA	17.145	NA
52	NA	NA	NA	16.120	NA
61	NA	NA	NA	15.011	NA
62	NA	NA	NA	13.340	NA
91	NA	NA	NA	13.460	NA
92	NA	NA	NA	16.000	NA
101	26.800	26.770	NA	NA	NA
103	31.440	31.330	NA	31.350	NA
104	NA	30.230	NA	30.250	NA
105	NA	26.880	NA	26.890	NA
106	24.370	NA	NA	NA	NA
107	NA	NA	NA	NA	15.500
108	NA	NA	NA	NA	14.470
109	NA	NA	NA	NA	11.860
110	NA	NA	NA	NA	11.530
111	NA	NA	NA	NA	11.615
112	NA	NA	NA	NA	11.840
113	NA	NA	NA	NA	11.840
114	NA	NA	10.400	10.380	NA
115	NA	NA	10.380	10.350	NA
116	25.380	25.340	NA	NA	NA
118	25.700	NA	NA	NA	NA
119	24.120	24.370	NA	NA	NA
120	NA	25.420	NA	25.430	NA
121	28.600	28.540	NA	NA	NA
122	21.660	NA	21.650	NA	21.695
123	21.560	NA	20.920	NA	21.040
124	20.570	NA	NA	NA	20.595
125	NA	19.610	NA	NA	19.750
126	NA	16.470	NA	NA	16.690
128	NA	NA	NA	11.790	NA

Depths to water in feet

	date				
piez. code	10/2/87	10/23/87	10/24/87	11/3/87	11/6/87
132	NA	19.100	NA	NA	19.235
133	NA	19.030	NA	NA	19.175
134	20.920	NA	20.860	NA	20.970
135	20.610	NA	20.540	NA	20.645
136	20.500	NA	20.440	NA	20.530
137	22.240	NA	21.900	NA	21.695
138	22.560	NA	21.930	NA	22.015
139	22.540	NA	21.900	NA	21.980
140	NA	NA	NA	NA	16.740
141	NA	16.700	NA	NA	16.850
142	NA	16.780	NA	NA	16.930
143	NA	NA	NA	NA	14.665
148	26.200	NA	NA	NA	NA
172	NA	16.620	NA	NA	16.775
175	NA	NA	NA	NA	15.140
176	NA	NA	NA	NA	11.570
177	21.430	NA	21.430	NA	21.490
178	20.870	NA	20.860	NA	20.940
179	NA	19.660	NA	NA	19.805
180	NA	NA	11.890	11.590	NA
181	NA	NA	11.610	11.610	NA
440	NA	NA	NA	NA	20.650
722	NA	NA	NA	11.595	NA

APPENDIX 5: PIEZOMETER DATA USED IN STUDY

The following piezometers are the shallowest ones in their respective piezometer nests and were called observation wells in this study. The water table elevations shown are given by the measuring point elevation minus the depth to water in the piezometer (observed on the date closest to the first week in November, 1987); these values were used to produce the map in Figure 14. Of these 27 observation wells, 21 are next to roads where GPR surveys have been performed and serve as calibrating wells for the GPR data. For these 21 the depth of water below the road surface has been calculated from the water table depth in the piezometer and the difference in elevation between the measuring point of the piezometer and the road surface.

piez. code	mi. E of County F	mi. N of Birch St.	WT elevation (ft asl)	depth of WT below road (ft)
722	0.00	1.00	1053.705	10.277
101	0.85	2.20	1038.030	
116	1.05	2.55	1036.960	
119	1.20	2.30	1042.230	
122	1.25	2.00	1046.705	20.120
118	1.25	2.50	1039.100	
126	1.50	1.50	1053.410	14.878
123	1.50	2.00	1048.160	19.919
120	1.50	2.45	1043.270	24.717
104	1.50	2.85	1036.650	29.355
111	1.60	1.00	1055.885	10.401
124	1.75	2.00	1049.505	19.839
106	1.75	2.40	1044.630	
112	2.00	0.65	1055.860	9.618
108	2.00	1.50	1055.330	14.004
440	2.00	2.00	1051.650	17.962
1	2.00	2.25	1048.930	22.225
3	2.00	2.50	1043.780	
125	2.35	2.25	1051.290	17.972
115	2.85	1.00	1058.750	9.159
128	2.85	1.50	1058.010	11.209
61	2.85	1.75	1057.789	11.651
31	2.85	2.25	1056.118	15.030
5	2.85	2.40	1054.535	16.231
12	2.85	2.60	1052.850	17.469
92	3.05	2.25	1055.200	14.166
51	3.30	2.25	1056.855	14.057

APPENDIX 6: GPR SURVEY DATA

All radar survey data analyzed in this study were obtained during the first week of November, 1987. Below are radar survey results ordered by miles east of Portage County Highway F, miles north of Birch Avenue and survey number. As an example of the survey number convention, 114.2 is the second survey performed on 11/4/87. There are replicate values at most radar survey points. All data shown were obtained with an antenna with a center frequency of 80 MHz.

mi. E of County F	mi. N of Birch St.	survey number	water table return time (ns)
0.00	1.00	114.4	40.8900
0.05	1.00	114.4	37.4825
0.10	1.00	114.4	42.2530
0.15	1.00	114.4	47.4324
0.20	1.00	114.4	50.4310
0.25	1.00	114.4	49.0680
0.30	1.00	113.1	52.9560
0.30	1.00	114.4	49.7495
0.35	1.00	113.1	49.7198
0.35	1.00	114.4	46.3420
0.40	1.00	113.1	53.9857
0.40	1.00	114.4	48.3865
0.45	1.00	113.1	52.9560
0.45	1.00	114.4	45.6605
0.50	1.00	113.1	50.0140
0.50	1.00	114.4	47.0235
0.55	1.00	113.1	53.5444
0.55	1.00	114.4	44.2975
0.60	1.00	114.4	47.0235
0.65	1.00	114.4	46.3420
0.65	2.00	113.2	125.0350
0.70	1.00	114.4	47.0235
0.70	2.00	113.1	125.7705
0.75	1.00	113.1	42.0706
0.75	1.00	114.4	49.0680
0.75	2.00	113.2	107.3830
0.80	1.00	113.1	40.0112
0.80	1.00	114.4	41.5715
0.80	2.00	113.1	111.0605
0.85	1.00	113.1	42.0706
0.85	1.00	114.4	41.5715
0.85	2.00	113.2	104.4410
0.90	1.00	114.4	45.6605
0.90	2.00	113.1	104.4410
0.95	1.00	113.1	42.3648

mi. E of County F	mi. N of Birch St.	survey number	water table return time (ns)
1.00	1.00	113.1	46.7778
1.00	1.00	114.4	42.2530
1.00	2.00	113.1	108.8540
1.05	1.00	113.1	41.0409
1.05	1.00	114.4	38.1640
1.05	2.00	113.2	97.8215
1.10	1.00	114.4	47.7050
1.10	2.00	113.1	98.8512
1.15	1.00	113.1	48.2488
1.15	1.00	114.4	43.6160
1.15	2.00	113.2	85.3180
1.20	1.00	113.1	46.6307
1.20	1.00	114.4	38.1640
1.20	2.00	113.1	89.7310
1.25	1.00	113.1	45.0126
1.25	1.00	114.4	38.1640
1.25	2.00	113.2	86.7890
1.30	1.00	113.1	39.4228
1.30	1.00	114.4	42.2530
1.30	2.00	113.1	88.2600
1.35	1.00	114.4	43.6160
1.35	2.00	113.2	88.2600
1.40	1.00	113.1	33.9801
1.40	1.00	114.4	42.9345
1.40	2.00	113.1	88.2600
1.45	1.00	113.1	32.2149
1.45	1.00	114.4	44.9790
1.45	2.00	113.2	86.7890
1.50	1.00	113.1	30.7439
1.50	1.00	114.4	43.6160
1.50	1.00	114.5	44.9790
1.50	1.05	114.5	43.6160
1.50	1.10	114.5	47.0235
1.50	1.15	114.5	43.6160
1.50	1.20	114.5	44.9790
1.50	1.25	114.5	54.5200
1.50	1.30	114.5	57.9275
1.50	1.35	114.5	57.2460
1.50	1.40	114.5	64.7425
1.50	1.45	114.5	66.7870
1.50	1.50	114.5	62.0165
1.50	1.55	114.5	63.3795
1.50	1.60	114.5	65.4240
1.50	1.65	114.5	64.0610
1.50	1.70	114.5	66.7870

mi. E of County F	mi. N of Birch St.	survey number	water table return time (ns)
1.50	1.75	114.5	69.5130
1.50	1.80	114.5	68.8315
1.50	1.85	114.5	73.6020
1.50	1.90	114.5	73.6020
1.50	1.95	114.5	79.0540
1.50	2.00	113.1	87.5245
1.50	2.00	113.2	79.4340
1.50	2.00	114.5	84.5060
1.50	2.05	114.5	87.9135
1.50	2.10	114.5	93.3655
1.50	2.15	114.5	92.6840
1.50	2.45	114.5	105.6325
1.50	2.50	114.5	107.6770
1.50	2.55	114.5	109.0400
1.50	2.60	114.5	111.7660
1.50	2.65	114.5	114.4920
1.50	2.70	114.5	112.4475
1.50	2.75	114.5	110.4030
1.50	2.80	114.5	121.9885
1.50	2.85	114.5	129.4850
1.55	1.00	114.4	43.6160
1.55	2.00	113.1	90.4665
1.60	1.00	113.1	30.4497
1.60	1.00	114.4	38.1640
1.60	2.00	113.1	80.9050
1.60	2.00	113.2	79.7282
1.65	1.00	113.1	30.1555
1.65	1.00	114.4	38.1640
1.65	2.00	113.1	79.4340
1.65	2.00	113.2	80.1695
1.70	1.00	114.4	42.2530
1.70	2.00	113.1	77.9630
1.70	2.00	113.2	80.9050
1.75	1.00	113.1	29.4200
1.75	1.00	114.4	40.8900
1.75	2.00	113.1	80.9050
1.75	2.00	113.2	83.8470
1.80	1.00	113.1	27.9490
1.80	1.00	114.4	36.8010
1.80	2.00	113.1	84.4354
1.80	2.00	113.2	83.8470
1.85	1.00	114.4	40.2085
1.85	2.00	113.1	83.8470
1.85	2.00	113.2	79.4340
1.90	1.00	113.1	29.4200

mi. E of County F	mi. N of Birch St.	survey number	water table return time (ns)
1.90	1.00	114.4	42.2530
1.90	2.00	113.1	79.4340
1.90	2.00	113.2	79.4340
1.95	1.00	113.1	30.8910
1.95	1.00	114.4	40.8900
1.95	2.00	113.1	82.3760
2.00	0.0	114.3	16.3560
2.00	0.05	114.3	21.8080
2.00	0.10	114.3	27.2600
2.00	0.15	114.3	34.0750
2.00	0.20	114.3	34.7565
2.00	0.25	114.3	38.1640
2.00	0.30	114.3	39.5270
2.00	0.35	114.3	32.7120
2.00	0.40	114.3	34.0750
2.00	0.45	114.3	36.8010
2.00	0.50	114.3	36.8010
2.00	0.55	114.3	34.7565
2.00	0.60	114.3	34.7565
2.00	0.65	114.3	32.7120
2.00	0.70	114.3	38.8455
2.00	0.75	114.3	34.7565
2.00	0.80	114.3	35.4380
2.00	0.85	114.3	34.0750
2.00	0.90	114.3	36.8010
2.00	0.95	114.3	39.5270
2.00	1.00	113.1	39.7170
2.00	1.00	114.3	39.5270
2.00	1.00	114.4	39.5270
2.00	1.05	113.1	34.8627
2.00	1.05	114.3	39.5270
2.00	1.10	114.3	48.3865
2.00	1.15	114.3	48.3865
2.00	1.20	114.3	53.1570
2.00	1.25	114.3	53.1570
2.00	1.30	114.3	54.5200
2.00	1.35	113.1	58.8400
2.00	1.35	114.3	56.8371
2.00	1.40	113.1	55.1625
2.00	1.40	114.3	54.2474
2.00	1.45	113.1	58.8400
2.00	1.45	114.3	53.1570
2.00	1.50	113.1	60.3110
2.00	1.50	114.3	58.6090
2.00	1.55	113.1	46.9249

mi. E of County F	mi. N of Birch St.	survey number	water table return time (ns)
2.00	1.55	114.3	63.3795
2.00	1.60	113.1	58.8400
2.00	1.60	114.3	63.3795
2.00	1.65	113.1	69.5783
2.00	1.65	114.3	64.0610
2.00	1.70	113.1	68.6957
2.00	1.70	114.3	68.8315
2.00	1.75	114.3	74.9650
2.00	1.80	113.1	74.1384
2.00	1.80	114.3	71.5575
2.00	1.85	113.1	73.5500
2.00	1.85	114.3	68.8315
2.00	1.90	113.1	70.6080
2.00	1.90	114.3	70.8760
2.00	1.95	113.1	71.9319
2.00	1.95	114.3	79.7355
2.00	2.00	113.1	75.3152
2.00	2.00	113.2	77.9630
2.00	2.00	114.3	84.5060
2.00	2.05	114.3	85.8690
2.00	2.10	114.3	91.3210
2.00	2.15	114.3	93.3655
2.00	2.20	114.3	96.7730
2.00	2.25	114.3	91.3210
2.05	1.00	114.4	42.2530
2.05	2.25	114.3	84.5060
2.10	1.00	114.4	42.9345
2.10	2.25	114.3	92.6840
2.15	1.00	114.4	39.5270
2.15	2.25	114.3	84.5060
2.20	1.00	114.4	42.2530
2.20	2.25	114.3	83.1430
2.25	1.00	114.4	42.5256
2.25	2.25	114.3	83.1430
2.30	1.00	114.4	40.8900
2.30	2.25	114.3	80.4170
2.35	1.00	114.4	39.5270
2.35	2.25	114.3	74.9650
2.40	1.00	114.4	42.1167
2.40	2.25	114.3	76.7369
2.45	1.00	114.4	42.2530
2.45	2.25	114.3	70.8760
2.50	1.00	114.4	39.2544
2.50	2.25	114.3	72.2390
2.55	1.00	114.4	39.5270

mi. E of County F	mi. N of Birch St.	survey number	water table return time (ns)
2.55	2.25	114.3	71.5575
2.60	1.00	114.4	42.9345
2.60	2.25	114.3	70.8760
2.65	1.00	114.4	38.7092
2.65	2.25	114.3	72.2390
2.70	1.00	114.4	37.4825
2.70	2.25	114.3	68.8315
2.75	1.00	114.4	34.7565
2.75	2.25	114.3	61.3350
2.80	1.00	114.4	36.8010
2.80	2.25	114.3	61.3350
2.85	0.0	114.3	14.3115
2.85	0.05	114.3	10.2225
2.85	0.10	114.3	14.3115
2.85	0.15	114.3	10.2225
2.85	0.20	114.3	20.4450
2.85	0.25	114.3	19.0820
2.85	0.30	114.3	10.9040
2.85	0.35	114.3	17.7190
2.85	0.40	114.3	29.5771
2.85	0.45	114.3	27.2600
2.85	0.50	114.3	29.9860
2.85	0.55	114.3	29.9860
2.85	0.60	114.3	30.6675
2.85	0.65	114.3	27.2600
2.85	0.70	114.3	29.9860
2.85	0.75	114.3	27.9415
2.85	0.80	114.3	33.1209
2.85	0.85	114.3	32.7120
2.85	0.90	114.3	36.3921
2.85	0.95	114.3	35.4380
2.85	1.00	114.2	41.3700
2.85	1.00	114.3	39.5270
2.85	1.00	114.4	36.8010
2.85	1.05	114.2	38.6120
2.85	1.05	114.3	38.1640
2.85	1.10	114.2	39.9910
2.85	1.10	114.3	34.0750
2.85	1.15	114.2	39.9910
2.85	1.15	114.3	36.8010
2.85	1.20	114.2	35.1645
2.85	1.20	114.3	38.1640
2.85	1.25	114.3	39.5270
2.85	1.30	114.2	38.6120
2.85	1.30	114.3	36.8010

mi. E of County F	mi. N of Birch St.	survey number	water table return time (ns)
2.85	1.35	114.2	39.9910
2.85	1.35	114.3	39.5270
2.85	1.40	114.2	40.2668
2.85	1.40	114.3	40.2085
2.85	1.45	114.2	39.5773
2.85	1.45	114.3	39.5270
2.85	1.50	114.2	46.4723
2.85	1.50	114.3	44.2975
2.85	1.55	114.2	46.8860
2.85	1.55	114.3	46.3420
2.85	1.60	114.3	44.2975
2.85	1.65	114.2	43.4385
2.85	1.65	114.3	42.2530
2.85	1.70	114.3	42.2530
2.85	1.75	114.2	48.2650
2.85	1.75	114.3	47.7050
2.85	1.80	114.3	48.3865
2.85	1.85	114.3	47.7050
2.85	1.90	114.3	49.0680
2.85	1.95	114.3	54.5200
2.85	2.00	114.3	43.6160
2.85	2.05	114.3	59.2905
2.85	2.10	114.3	66.7870
2.85	2.15	114.3	59.9720
2.85	2.20	114.3	66.7870
2.85	2.25	114.2	64.8130
2.85	2.25	114.3	65.4240
2.85	2.25	114.3	66.1055
2.85	2.30	114.2	68.9500
2.85	2.30	114.3	67.4685
2.85	2.35	114.2	66.1920
2.85	2.35	114.3	69.5130
2.85	2.40	114.2	68.2605
2.85	2.40	114.3	62.6980
2.85	2.45	114.2	75.8450
2.85	2.45	114.3	68.8315
2.85	2.50	114.2	77.2240
2.85	2.50	114.3	72.9205
2.85	2.55	114.2	75.1555
2.85	2.55	114.3	75.6465
2.85	2.60	114.2	78.6030
2.85	2.60	114.3	76.3280
2.85	2.65	114.2	88.2560
2.85	2.65	114.3	82.4615
2.85	2.70	114.2	82.7400

mi. E of County F	mi. N of Birch St.	survey number	water table return time (ns)
2.85	2.70	114.3	81.7800
2.85	2.75	114.3	74.9650
2.85	2.80	114.2	81.6368
2.85	2.80	114.3	85.8690
2.85	2.85	114.2	86.8770
2.85	2.85	114.3	80.4170
2.85	2.90	114.2	81.7747
2.85	2.90	114.3	89.9580
2.85	2.95	114.2	58.6075
2.85	2.95	114.3	77.6910
2.85	3.00	114.2	81.3610
2.85	3.00	114.3	77.0095
2.85	3.05	114.2	107.5620
2.85	3.05	114.3	94.0470
2.85	3.10	114.2	114.4570
2.85	3.10	114.3	110.4030
2.85	3.15	114.2	113.0780
2.85	3.15	114.3	115.1735
2.85	3.20	114.2	92.3930
2.85	3.20	114.3	104.9510
2.85	3.25	114.2	89.6350
2.85	3.25	114.3	92.6840
2.85	3.30	114.2	107.5620
2.85	3.30	114.3	89.9580
2.90	1.00	114.4	35.4380
2.90	2.25	114.3	67.4685
2.95	1.00	114.4	37.4825
2.95	2.25	114.3	62.6980
3.00	1.00	114.4	38.1640
3.00	2.25	114.3	55.8830
3.05	1.00	114.4	36.8010
3.05	2.25	114.3	63.3795
3.10	1.00	114.4	36.8010
3.10	2.25	114.3	53.8385
3.15	1.00	114.4	32.7120
3.15	2.25	114.3	57.2460
3.20	1.00	114.4	28.6230
3.20	2.25	114.3	61.3350
3.25	1.00	114.4	30.6675
3.25	2.25	114.3	61.3350
3.30	1.00	114.4	35.4380
3.30	1.05	114.4	33.3935
3.30	1.10	114.4	35.4380
3.30	1.15	114.4	35.4380
3.30	1.20	114.4	39.5270

mi. E of County F	mi. N of Birch St.	survey number	water table return time (ns)
3.30	1.25	114.4	38.1640
3.30	1.30	114.4	40.8900
3.30	1.35	114.4	38.1640
3.30	1.40	114.4	38.1640
3.30	1.45	114.4	37.4825
3.30	1.50	114.4	40.8900
3.30	1.55	114.4	39.5270
3.30	1.60	114.4	40.2085
3.30	1.65	114.4	42.2530
3.30	1.70	114.4	47.7050
3.30	1.75	114.4	47.7050
3.30	1.80	114.4	49.0680
3.30	1.85	114.4	53.1570
3.30	1.90	114.4	51.7940
3.30	1.95	114.4	54.5200
3.30	2.25	114.3	50.8399

231763 - A Ground Penetrating Radar Study of Water Table Elevation in a Portion of Wisconsin's Central Sand Plain.